学位論文

Description of Fermionic Wavefunctions by Symmetric Tensor Decomposition (対称テンソル分解によるフェルミ粒子系の波動関数の記述)

平成２５年１２月博士 (理学) 申請

東京大学大学院理学系研究科
物理学専攻
植村　渉

Abstract

There are a number of evidences and findings in quantum electronic systems in the last a few decades, such as the high Tc superconductivity in cuprates and the colossal magnetoresistance in perovskite oxides, etc. Much effort has been paid to understand the variety of challenging phenomena in condensed matter physics, but we still lack a unified and indisputable theoretical framework that can explain and predict most of these experimental facts.

The situation of the theoretical understanding for quantum many body systems has been much refreshed after the discovery of Density Matrix Renormalization Group (DMRG) method in 1992. Since then, numerical and mathematical researches in the so called tensor network frameworks have attracted considerable attention. We focus on theoretical and numerical approaches toward the tensor network framework that make use of quantum information theory and are applicable to quantum chemistry. The purpose of this thesis is to give a tensor network framework that explicitly considers the antisymmetry of the electronic wavefunction contrary to most of the previous works. With a proper consideration of the antisymmetry of the wavefunction, we can dramatically reduce the number of states constituting the total wavefunction and improve the speed of numerical calculation and enhance the convergence of the resulting energy.

In chapter 3, we introduce our recently published wavefunction theory where tensor network of the wavefunction is treated using the symmetric tensor decomposition framework with the antisymmetry of the wavefunction explicitly taken into account. This scheme is based on the configuration interaction (CI) which is a versatile wavefunction theory for interacting fermions but involving an extremely long CI series. Using a symmetric tensor decomposition (STD) method, we convert the CI series into a compact and numerically tractable form. The converted series encompasses the Hartree-Fock state in the first term and rapidly converges to the full-CI state, as numerically tested using small

molecules. Provided that the length of the STD-CI series grows only moderately with the increasing complexity of the system, the new method will serve as one of the alternative variational methods to achieve full-CI with enhanced practicability.

In Chapter 4, we introduce an improvement of STD-CI. In the Extended STD (ESTD) scheme, the variational degree of freedom in the wavefunction is dramatically extended. Therefore we can expect a considerable improvement in the convergence of the energy in ESTD. And also, in ESTD we can calculate the expectation value of the energy and the first derivatives with a calculation cost proportional to N^5, while the original scaling in STD-CI is N^6, where N is the number of electrons. This immediately means that we can dramatically extend the size of the systems that we can treat with ESTD, compared with STD-CI. In ESTD, the wavefunction is given as a linear combination of the Antisymmetrized Geminal Powers (AGP), and the norm and energy are given through a simple formalism based on Pfaffian. We provide a comparison of numerical results of the water molecule and the Hubbard model that indicates the numerical superiority of ESTD with respect to STD-CI. In future we expect to treat larger systems with ESTD, including three dimensional periodic systems. Such calculations will be propelled by the fact that in ESTD we can treat non orthogonal basis sets without taking orthonormalization, which is a procedure that significantly complicates large-scale calculations.

Contents

Chapter 1

Introduction

There are many interesting and challenging phenomena in many body electronic systems. To name a few, high Tc superconductivity in cuprate systems, colossal magnetoresistance in perovskite oxides, quantum hall effect on gallium arsenides, topologically ordered phases, quantum spin liquids, etc. As there are many experimental evidences and findings in condensed matter physics in the last a few decades, there exist a small number of theoretical integrated frameworks that can explain and predict most part of these variety of phenomena in a coherent and indisputable way. There should be further a room for theoretical efforts to establish a clear and unified way of understanding these, beyond the imperfectness of the theories of our semi classical milestones, one of those being the Density functional theory (DFT) based on the Local Density Approximation (LDA).

The situation of theoretical framework for correlated quantum many body systems has much been refreshed by the discovery of the Density Matrices Renormalization Group (DMRG) theory(White, 1992)[1, 2], one of its success reached the theoretical estimation of the ground state energy of isotropic $S = 1$ Heisenberg chain model as $E_0 = -1.401484038971(4)$ per site, that can be regarded as the accuracy limit of the machine precision. There are few established numerical techniques beyond the analytic treatment of the quantum systems that can reproduce this level of numerical accuracy other than DMRG.

Almost one decade after the establishment of the DMRG technique, it was clarified that for one dimensional (1D) gapped quantum systems, DMRG can faithfully reproduce the exact ground states, where the entanglement entropy scales as a constant with respect to the system size(Verstraete et al, 2006)[3]. Thus, with the aid of the recently emerging developments in quantum information theory, we can find a mathematical justification to rely on the DMRG and a wide variety of algorithmic extensions of it on the examination of the behavior of quantum many body systems.

We can use the well-established DMRG codes for the description of 1D or possibly 2D quantum lattice models. DMRG method is regarded to require computational resources that scale polynomially with system size, as long as the target system satisfies some physical conditions, such as the linear shape of correlation structure of the system and absence of no quantum criticality in the system, etc. In those cases, DMRG does not suffer from the well-known exponential computation hardness as do the exact diagonalization techniques(ED) such as the Lanczos method or the Davidson method. And also, DMRG does not suffer from the sign problem of fermionic systems, that severely hampers numerical application of another well-established technique, namely the quantum Monte

Carlo method(QMC).

The application of DMRG to quantum chemical systems started almost after a decade of its foundation. In general chemical molecules, the sites in lattice models correspond to the molecular orbitals within the given basis set functions. In contrast to the 1D lattice systems, there is no natural ordering of molecular orbitals of chemical systems, so it is important to assume an efficient orbital ordering based on the strengths of the correlation between the orbitals(Chan and Head-Gordon, 2002)[4]. It was found further that the DMRG description behaves better if the original chemical system has the entanglement structure that is linearly extending. If there is no such structure in the target molecule, still we can construct a tensor tree network states (TTNS) as a simple generalization of the DMRG scheme (Nakatani and Chan, 2013)[5]. TTNS well captures the behavior of molecular systems particularly when there is tree like structure in the target molecule.

Though DMRG has many advantages as a theory for quantum many body systems in the language of the tensor network, we will point out that DMRG does not explicitly consider the antisymmetry of the total wavefunction in its basic formalism, when dealing with the systems composed of fermions. [1] There are, however, algorithms to explicitly make the wavefunction of electrons antisymmetric with respect to the permutation of any two electrons, with which to dramatically decrease the number of states of the total system by a factor of $N!$ where N is the number of electrons. If we can build a numerical tensor network formalism that explicitly represents the antisymmetry of the wavefunction, we can expect to have both considerable speedup of numerical iterations of the method and improved energy convergence towards the exact value in the sense of full CI, compared to the theory without antisymmetry.

In Chapter 3, we introduce the recently published wavefunction theory with the correct treatment of the antisymmetry of electronic wavefunctions, that is mainly based on the Symmetric Tensor Decomposition technique (Uemura and Sugino, 2012)[6]. This method (Symmetric Tensor Decomposition-Configuration Interaction, STD-CI) can be further extended to the theory of the linear combination of antisymmetrized geminal power (AGP) wavefunctions, which we explain in Chapter 4. When numerical problems of this last theory is overcome by future study, we can expect that this method (Extended Symmetric Tensor Decomposition, ESTD) can achieve very high numerical accuracy of the calculation of the total energy of the system within the computational time scaling as N^5. Such a theory is with no doubt competitive to a tensor network based framework for the description of correlated electronic systems and should be taken seriously.

[1]Typically DMRG is formulated using the number representation (second quantization) to describe the wavefucntion as an antisymmetric tensor product of orbitals multiplied by the coefficients as

$$\sum_{\mu_1=0}^{1} \cdots \sum_{\mu_M=0}^{1} U(\mu_1, \ldots \mu_M) e^{\mu_1} \otimes \cdots \otimes e^{\mu_M} \tag{1.1}$$

where M is the number of basis functions and e^{μ} is the canonical basis, $\{e^0 = |0\rangle, e^1 = |1\rangle\}$, searching therein the most efficient description of U (=tensor of rank M) [1]. Here the antisymmetry of the basis is decoupled from U throughout in the formulation, contrary to our scheme where the permutation tensor as well as the coefficient is decomposed into pieces to search for the efficiency. In this sense, the former is implicit and the latter is explicit in treating the antisymmetry of the wavefunction.

[1]See, for example, O. Legeza, T. Rohwedder, R. Schneider and S. Szalay, "Tensor Product Approximation (DMRG) and Coupled Cluster method in Quantum Chemistry", arXiv:1310.2736 [physics.chem-ph].

Chapter 2

Background

2.1 Formalism of DMRG based on Matrix Product States

In this section, we briefly overview the formalism of DMRG using the language of Matrix Product States(MPS). Though there are bulk of papers introducing the basic formalism of DMRG, we choose one of them (Nakatani and Chan, 2013)[5] to make a review on that basis. The MPS state can be constructed from left and right matrices (L, R) and state ψ,

$$|\Psi\rangle = \sum_{n_1 \cdots n_k} L^{n_1} \cdots L^{n_{i-1}} \psi^{n_i} R^{n_{i+1}} \cdots R^{n_k} |n_1 \cdots n_k\rangle . \tag{2.1}$$

Here the dimension of matrices L, R and ψ is set to M. Note that k is the number of sites and n_i is the number of states (= many-body bases) at site i. To remove the invariance under the matrix transformation, we assume following conditions,

$$\sum_{n_i} L^{n_i \dagger} L^{n_i} = 1, \tag{2.2}$$

$$\sum_{n_i} R^{n_i} R^{n_i \dagger} = 1. \tag{2.3}$$

Left and right kets $|l_{i-1}\rangle$ and $|r_i\rangle$ are constructed as

$$|l_{i-1}\rangle = \sum_{n_1 \cdots n_{i-1}} L^{n_1} \cdots L^{n_{i-1}} |n_1 \cdots n_{i-1}\rangle , \tag{2.4}$$

$$|r_i\rangle = \sum_{n_{i+1} \cdots n_k} R^{n_{i+1}} \cdots R^{n_k} |n_{i+1} \cdots n_k\rangle . \tag{2.5}$$

From the orthonormality of left and right matrices, we can say that these kets are orthonormal,

$$\left\langle l_{i-1} \middle| l'_{i-1} \right\rangle = \delta_{ll'}, \tag{2.6}$$

$$\langle r_i | r'_i \rangle = \delta_{rr'}. \tag{2.7}$$

From these ket states, we can construct the canonical DMRG form as $|l_{i-1}\rangle$ and $|r_i\rangle$,

$$|\Psi\rangle = \sum_{l_{i-1} n_i r_i} \psi^{n_i}_{l_{i-1} r_i} |l_{i-1} n_i r_i\rangle . \tag{2.8}$$

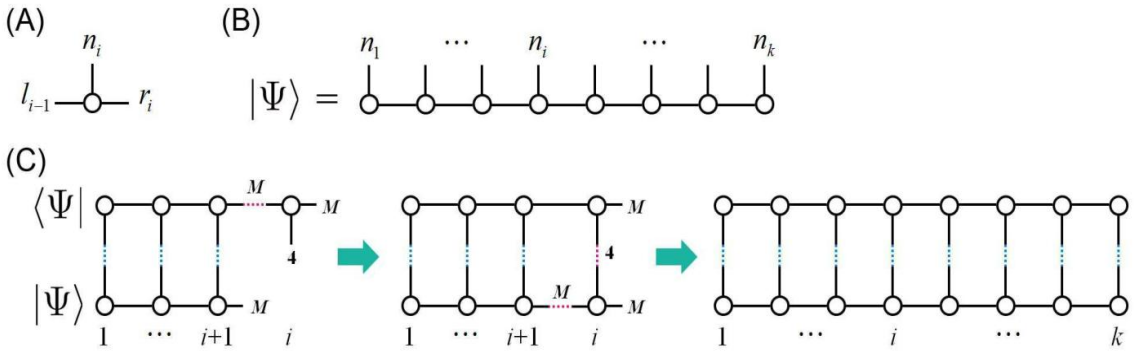

Figure 2.1: Graphical representations of MPS.[5] (A) one site coefficient vector ψ^{n_i} is a rank 3 tensor. (B)The MPS wavefunction is given by contracting all horizontal bonds, (C) The overlap of two MPS wavefunctions can be efficiently computed recursively.

We use tensor contraction technique in the computation of MPS. Figure 2.1 shows a graphical representation of the tensor contractions. With the technique, we can obtain the MPS wavefunction by contracting the horizontal edges in Fig. 2.1(B), whereby yielding the result as in (2.1). The technique also provides a way to compute the overlap of two MPS as shown in Fig. 2.1(C).

To determine the parameters, we minimize the MPS expectation energy for the Lagrangian

$$\left\langle \Psi \middle| \hat{H} \middle| \Psi \right\rangle - (\lambda \langle \Psi | \Psi \rangle - 1) \tag{2.9}$$

with respect to the parameters of the MPS. The minimization is carried out with respect to a single parameter for site by site at each step. In doing so, the MPS is expressed in the DMRG form (2.8) in i-th step of the DMRG sweep, and the coefficient vector ψ is optimized. The energy is a quadratic in ψ, therefore the minimization leads to an eigenvalue problem,

$$\sum_{l'_{i-1} n'_i r' i} \left\langle l_{i-1} n_i r_i \middle| \hat{H} \middle| l'_{i-1} n'_i r'_i \right\rangle \psi^{n_i}_{l_{i-1} r_i} - \lambda \psi^{n_i}_{l_{i-1} r_i} = 0. \tag{2.10}$$

The procedure of obtaining the DMRG wavefunction is graphically represented as shown in Fig. 2.2.

2.2 Success of the original DMRG theory

Ref.[1] is the first paper of DMRG by Steve White and perhaps the most cited paper in the tensor network research field. In this paper, White reported the DMRG result on the ground state energies of infinite $S = \frac{1}{2}$ and $S = 1$ antiferromagnetic Heisenberg chains. The final result for the $S = 1$ ground state energy appears to be more than 2 orders of magnitude more accurate than the best available from Monte Carlo calculations in those days. Fig. 2.3 shows the reported Haldane gap by DMRG. Here the Haldane gap is defined as the gap between the lowest lying total spin $S_T = 2$ and $S_T = 1$ states. The

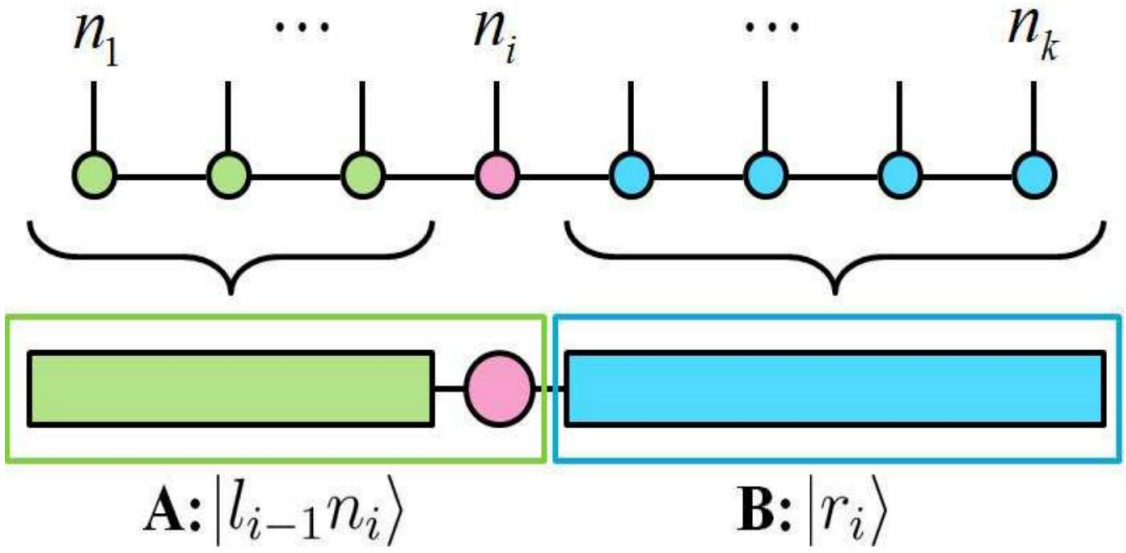

Figure 2.2: Graphical representations of DMRG wavefunction.[5] Canonical form of MPS wavefunction (top) can be rewritten as as block diagram in DMRG language (bottom).

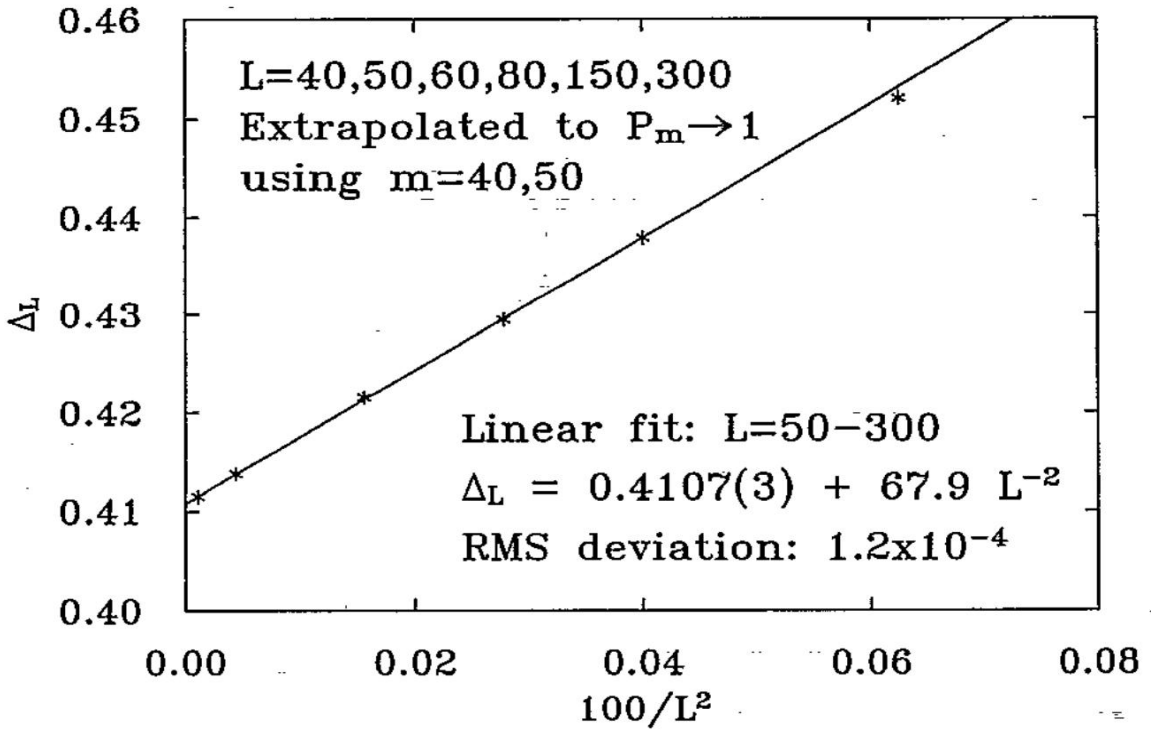

Figure 2.3: The Haldane gap as a functions of lattice size L[1].

data were fitted using the form

$$\Delta_L = \Delta + a/L^2 \tag{2.11}$$

with $\Delta = 0.4107(3)$ and $a = 67.9$. In contrast, the best Monte Carlo results for this gap was reported as $\Delta = 0.41$ in those days. Through comparison of these two results, we can clearly see the advantage of DMRG on 1D quantum lattice systems compared with Monte Carlo.

The first paper of DMRG by White was published on November 9, 1992 and in this version there are no detailed description on how to construct the DMRG code on the machine. In the succeeding paper in October 1, 1993, White published the algorithmic detail of the DMRG formalism.[2] This also is an important milestone in the early history of the development of DMRG and tensor network methods. In Table 2.1 and 2.2, we refer to those descriptions given by White.

Table 2.1: Infinite system density matrix algorithm for a 1D system. [2]

1. Make four initial blocks, each consisting of a single site, representing the initial four site system. Set up matrices representing the block Hamiltonian and other operators.
2. Form the Hamiltonian matrix (in sparse form) for the superblock.
3. Using the Davidson or Lanczos method, diagonalize the superblock Hamiltonian to find the target state $\psi(i_1, i_2, i_3, i_4)$. ψ is usually the ground state. Expectation values of various operators can be measured at this point using ψ.
4. Form the reduced density matrix for the two block system 1-2, using $\rho(i_1, i_2; i'_1, i'_2) = \sum_{i_3,i_4} \psi(i_1, i_2, i_3, i_4)\psi(i'_1, i'_2, i_3, i_4)$.
5. Diagonalize ρ to find a set of eigenvalues w_α and eigenvectors $u^\alpha_{i_1,i_2}$. Discard all but the largest m eigenvalues and associated eigenvectors.
6. Form matrix representations of operators (such as H) for the two block system 1-2 from operators for each separate block.
7. Form a new block 1 by changing basis to the u^α and truncating to m states using $H^{1'} = OH^{12}O^\dagger$, etc. If blocks 1 and 2 have m_1 and m_2 states, then O is an $m \times m_1 m_2$ matirx, with matrix elements $O(\alpha; i_1, i_2) = u^\alpha_{i_1,i_2}$, $\alpha = 1, \ldots, m$.
8. Replace old block 1 with new block 1.
9. Replace old block 4 with the reflection of new block 1.
10. Go to step 2.

In the succeeding paper of Steve White,[8] the research on the isotropic $S = 1$ Heisenberg chain was continued and unprecedented accuracy of a variety of properties was reported. The density matrix algorithms used in this paper give much more accurate results using open boundary conditions than with periodic boundary conditions. With periodic boundary conditions, each block has two ends which interact with the rest of the lattice, whereas with open boundary conditions, a block has only one active end if it contains either the right or left end of the chain. The effective Hamiltonian of the block must be made from a larger member of states if it must represent two active ends. It was possible to accurately reproduce bulk properties with open chains because they studied very large chains, up to several hundred sites. Table 2.3 shows the ground state energy

Table 2.2: Finite system density matrix algorithm for a 1D system consisting of L sites.[2] A calculation consists of several iterations, indexed by I, with each iteration consisting of $L-3$ steps, indexed by l, where l is the size of the first block.

1. (First half of $I=1$.) Use the infinite system algorithm for $L/2-1$ steps to build up the lattice to L sites. At each iteration store the block Hamiltonian and end operator matrices for block 1. Label the blocks by their size, B_l, $l=1,\ldots,L/2$.
2. (Start of second half of $I=1$.) Set $l=L/2$. Use B_l as block 1, and the reflection of B_{L-l-2} as block 4.
3. Steps 2-8 of Table 2.1.
4. Store the new block 1 as B_{l+1}, replacing the old B_{l+1}.
5. Replace block 4 with the reflection of B_{L-l-2}, obtained from the first half of this iteration.
6. If $l<L-3$, set $l=l+1$ and go to step 3.
7. (Start of iteration I, $I\geq 2$.) Make four initial blocks, the first three consisting of a single site, and the fourth consisting of the reflection of B_{L-3} from the previous iteration. Set $l=1$.
8. Steps 2-8 of Table 2.1.
9. Store the new block 1 as B_{l+1}, replacing the old B_{l+1}.
10. Replace block 4 with the reflection of B_{L-l-2}, obtained from the previous iteration (if $l\leq L/2-1$) or the first half of this iteration (if $l>L/2-1$).
11. If $l<L-3$, set $l=l+1$ and go to step 8. If $l=L-3$, start a new iteration by going to step 7. (Stop after 2 or 3 iterations.)

per site as a function of the number of states m. In these results, the reported ground state energy has the accuracy of almost machine precision.

2.3 Quantum Information Perspective of DMRG theory

In 2000s, DMRG was started to be studied in relation to the quantum information theory. In 2004, Verstraete et al. pointed out that there is a variational formulation of DMRG which allows dramatic improvements for the systems with periodic boundary conditions.[9] Let us briefly introduce the results of this paper. They have demonstrated that it is conceptually and algorithmically worthwhile to rephrase DMRG consistently in terms of matrix product states right from the beginning, thereby also abandoning the block concept.[10] Instead of providing detailed explanation, we just show Fig. 2.4 that sketches the concepts of Matrix Product States(MPS) description of DMRG schematically.

They also proposed the DMRG configurations for the case of periodic boundary conditions(Fig. 2.5). As a result of the improved algorithm of the DMRG on periodic boundary conditions, the energy convergence for periodic boundary conditions were much improved, thereby reaching the accuracy almost comparable to that of the open boundary conditions. See Fig. 2.6 for comparison.

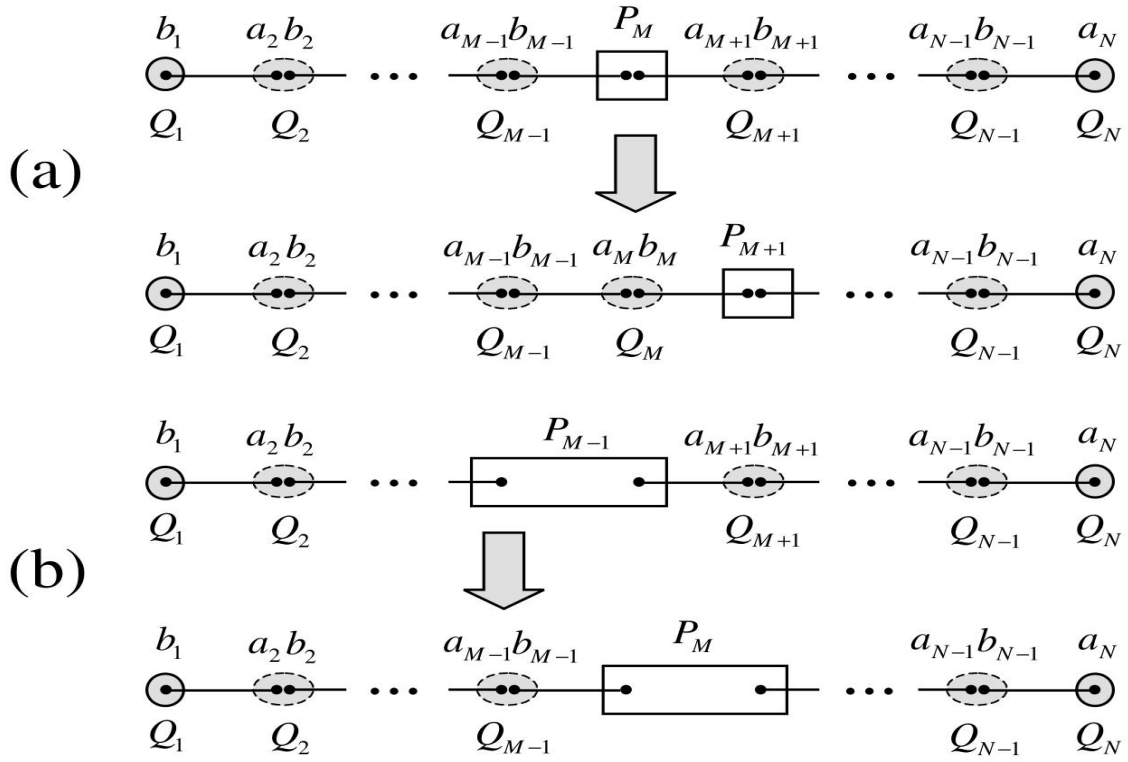

Figure 2.4: Schematic picture of the DMRG method for the $B \bullet B$ (a) and the $B \bullet\bullet B$ (b) configurations.[9] Horizontal lines represent maximally entangled states $|\phi\rangle$, the ellipses and circles (squares) the operators $Q(P)$ which map the auxiliary system into the physical ones.

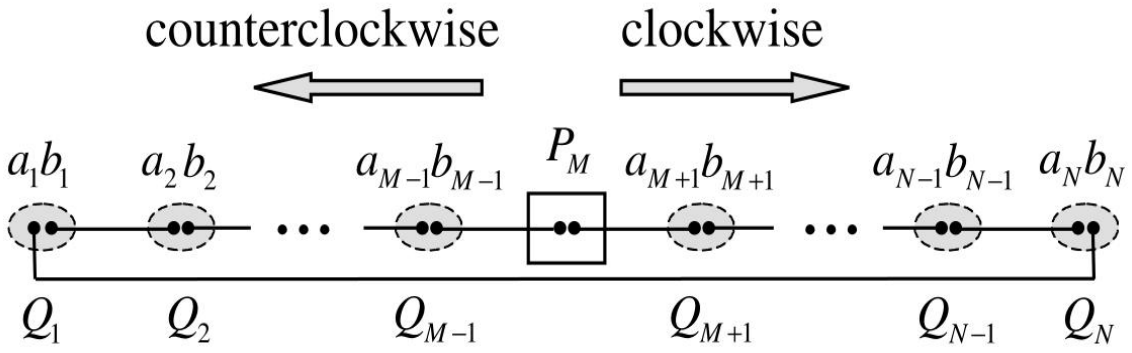

Figure 2.5: Proposed configurations for the case of periodic boundary conditions.[9] One may also use two spins instead of one.

Table 2.3: Ground state energy per site as a function of the number of states kept m.[8] The energy was obtained using the infinite lattice method, where the lattice size was increased until convergence of all digits shown was obtained. Also shown is the truncation error $1 - P(m)$.

m	e_0	$1 - P(m)$
36	-1.40148379810	5.61×10^{-8}
48	-1.40148401407	4.13×10^{-9}
60	-1.40148403106	1.23×10^{-9}
72	-1.40148403623	3.42×10^{-10}
86	-1.40148403729	1.34×10^{-10}
100	-1.40148403872	2.66×10^{-11}
110	-1.40148403887	1.27×10^{-11}
160	-1.401484038968	4.4×10^{-13}
180	-1.401484038970	1.4×10^{-13}

There are several reports that state the success of DMRG on 1D systems can be understood from the 1D area law of the entanglement entropy. [11, 12, 13, 14, 15, 16] The entropy of entanglement for the state $|\Psi_g\rangle$ is given by

$$S_L = -\mathrm{tr}(\rho_L \log_2 \rho_L), \tag{2.12}$$

where $\rho_L = \mathrm{tr}_{B_L} |\Psi_g\rangle \langle\Psi_g|$ is the reduced density matrix for B_L, a block of L spins in a 1D system.[13] For example, for the XX model with magnetic field, S_L can be numerically determined as

$$S_L^{XX} = \frac{1}{3}\log_2(L) + const. \tag{2.13}$$

up to $L = 100$ spins.[13] It was shown that MPS satisfies the "area law" of the entanglement entropy whose scaling is adapted to 1D systems. In more detail, it was shown that the entanglement entropy of a block of sites is bounded by a constant, more precisely $S(L) = -\mathrm{tr}(\rho_L \log \rho_L) = O(\log D)$, with ρ_L the reduced density matrix of the block.[17] This is exactly the same behavior that is usually observed in ground states of gapped 1D local Hamiltonians as we mentioned above. This is the main reason for the success of DMRG and MPS theory applied on gapped 1D systems.

However, when we go to 2D systems, the situation changes because in the entropy area law in 2D systems, the entropy scales as

$$S(L) \leq 4L \log D, \tag{2.14}$$

no more being constant with respect to the system size. The theory of projected entangled pair state (PEPS) was proposed [18] to give a proper tensor network description of 2D systems with the consideration of the area law of these systems. PEPS is a formulation of wavefunction based on the contraction of rank 4 tensors on the plane, as a graphical extension from MPS, that is a formulation based on the contraction of rank 2 tensors (matrices) on a line. Fig. 2.7 shows the graphical representation and entropy structure of PEPS. As we can see in Fig. 2.7, the boundary of the highlighted PEPS area has length

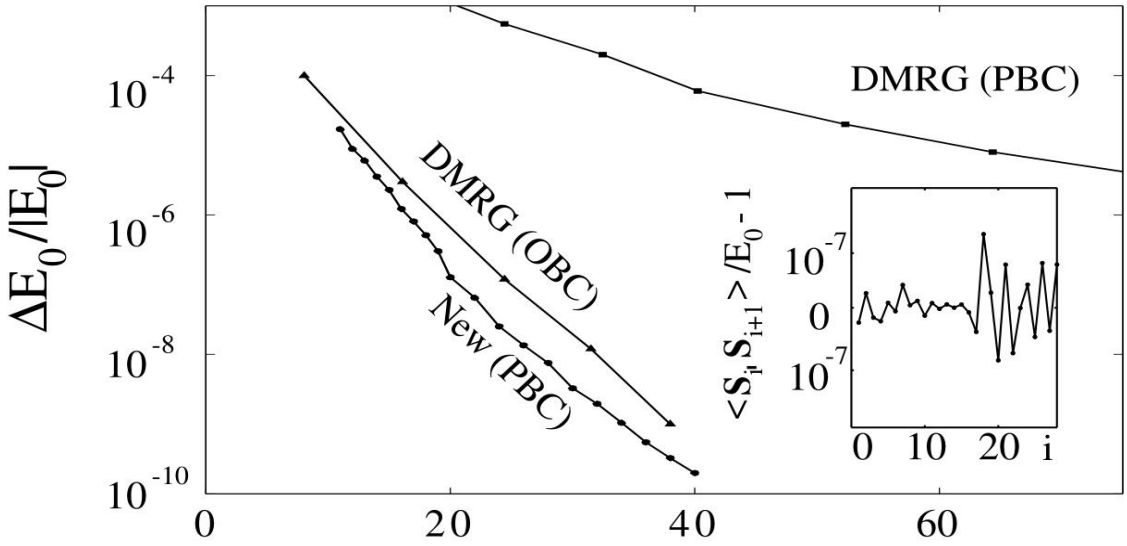

Figure 2.6: Left: comparison between DMRG (squares) [2] and the new method (circles) for periodic boundary conditions(PBC), and $N = 28$.[9] For reference the DMRG results [2] for the Heisenberg chain with open boundary conditions (OBC) (triangles) are also shown. Inset: variation of the local bond strength from the average along the chain, calculated with the new method and the bond dimension(D) = 40.

of $4L$, so this formulation can catch up the entropy scaling (2.14) for general 2D systems. However, it is known that the exact tensor contractions in PEPS formalism is in general an NP hard problem regarding the convergence with respect to the number of sites.[18]

2.4 DMRG in Quantum Chemistry

After a few years of the discovery of DMRG theory, DMRG was started to be systematically applied to quantum chemistry systems. We will focus on one of the DMRG chemistry paper, Chan and Head-Gordon(2002).[4] In quantum chemical systems, the situation for DMRG is different from 1D quantum lattice systems. Generally there are nothing like the 1D site ordering in quantum chemical systems. The nature of DMRG in quantum chemistry is such that the accuracy of the calculation depends both on the choice and ordering of the orbitals on the lattice. DMRG with bond dimension $M = 1$ will reproduce the Hatree Fock energy. For better accuracy, we should try to minimize the range of interactions of the Hamiltonian, so as to reduce the correlation length of the system. Chan and Head-Gordon chose a scheme to minimize the bandwidth of the integral matrix t_{ij} by reordering columns and rows. They found the symmetric reverse Cuthill McKee (RCM) reordering, [19, 20] which swaps columns and rows so as to make a sparse matrix more closely band diagonal, to be generally satisfactory. An example of a one electron integral reordering is shown in Fig. 2.8.

In this DMRG application on quantum chemical systems, the DMRG algorithm formally costs $O(M^2k^4) + O(M^3k^3)$ time per sweep, where M is the bond dimension and k is the number of orbitals. In Fig. 2.9, we refer to the plot of the sweep times for a series

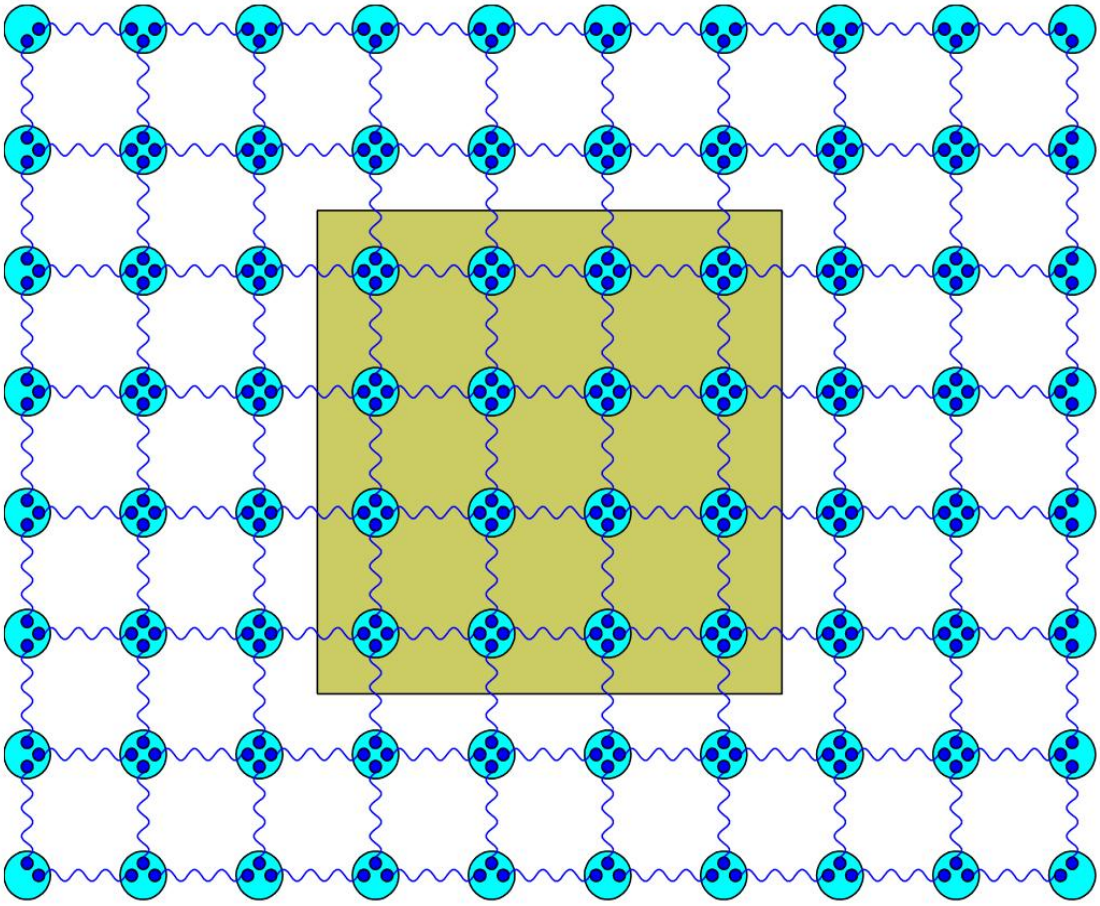

Figure 2.7: The entropy of a block of spins in a PEPS scales like the perimeter of the block: the Schmidt rank of the reduced density operator of the considered block of spins is bounded above by the product of the Schmidt ranks of the broken bonds.[18]

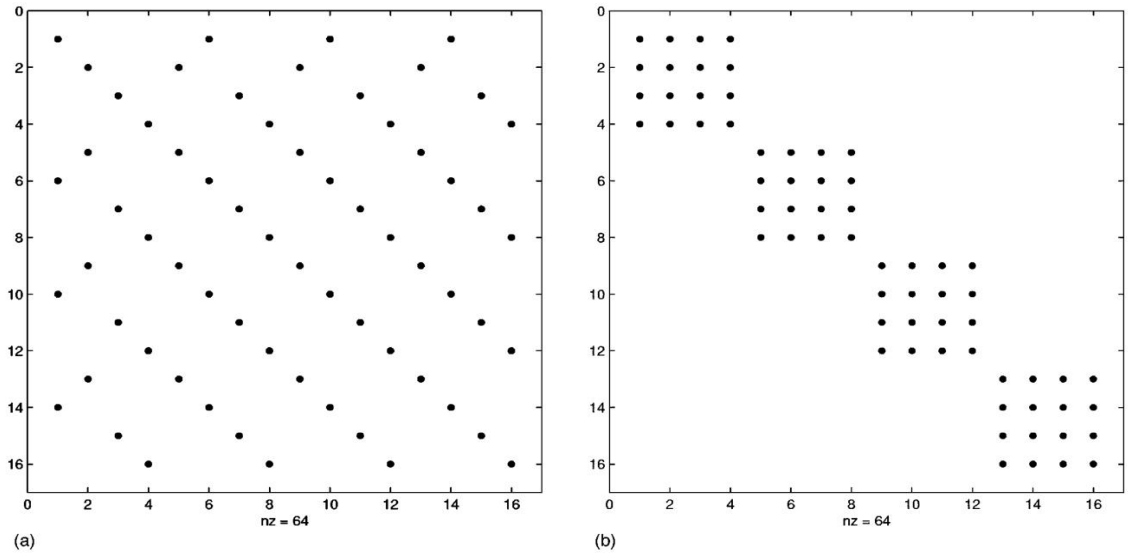

Figure 2.8: One electron integral matrices for a hydrogen chain.[4] (a) Integral matrix, when orbitals are ordered in the Hatree Fock energy ordering. (b) Integral matrix, after RCM reordering.

of calculations on the water molecule, with increasing M. We see that for the larger M values, the sweep times begin to display a cubic dependence on M.

The convergence of the DMRG energy as a function of $(\log M)^2$, to the full CI energy is shown in Fig. 2.10 and Table 2.4. These DMRG results are compared with coupled cluster theory, with perturbative triples (CCSD(T)) and perturbative triples and quadruples (CCSD(TQ)).[21] Using technology of those days, Chan and Head-Gordon were able to further extend those results to $M = 900$ yielding a final error of roughly 4μH. For this size of quantum chemical systems, they were able to achieve μH accuracy without too much effort. As can be seen from the table, already at $M \sim 400$, the DMRG is more accurate than even CCSD(TQ).

Chan and Head-Gordon stated in their conclusion that the cost of their most accurate DMRG calculations is considerably higher than that of CCSD(T) theory. They also observed that it became increasingly difficult to capture dynamic correlation in larger basis sets, because of the increasing range of the lattice Hamiltonian.

2.5 Pfaffian Wavefunctions with Quantum Monte Carlo

In Chapter 4, we will report on the results based on a theory with Antisymmetric Geminal Powers (AGP) and Pfaffian, as an alternative tensor-decomposition-based method. As a preparation we make a brief review on a few preceding researches that are related to APG and Pfaffian.[24, 25] For a system of $2N$ spin-polarized electrons the APG wavefunction is constructed as an antisymmetrized product of triplet pair orbitals $\chi(i,j) = -\chi(j,i)$ and is given by[22, 23]

$$\hat{A}[\chi(1,2)\chi(3,4)\ldots] = \mathrm{Pf}[\chi(i,j)] = \mathrm{Pf}[\xi], \tag{2.15}$$

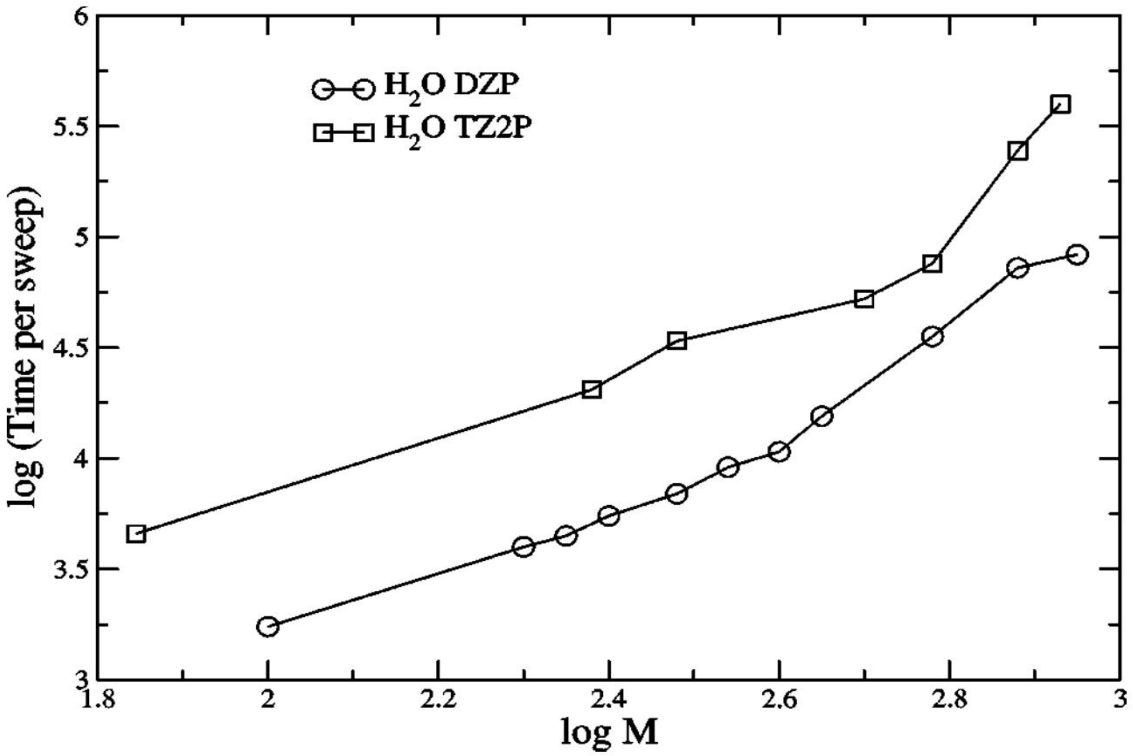

Figure 2.9: DMRG sweep time t as a function of the bond dimension M for a water calculation.[4]

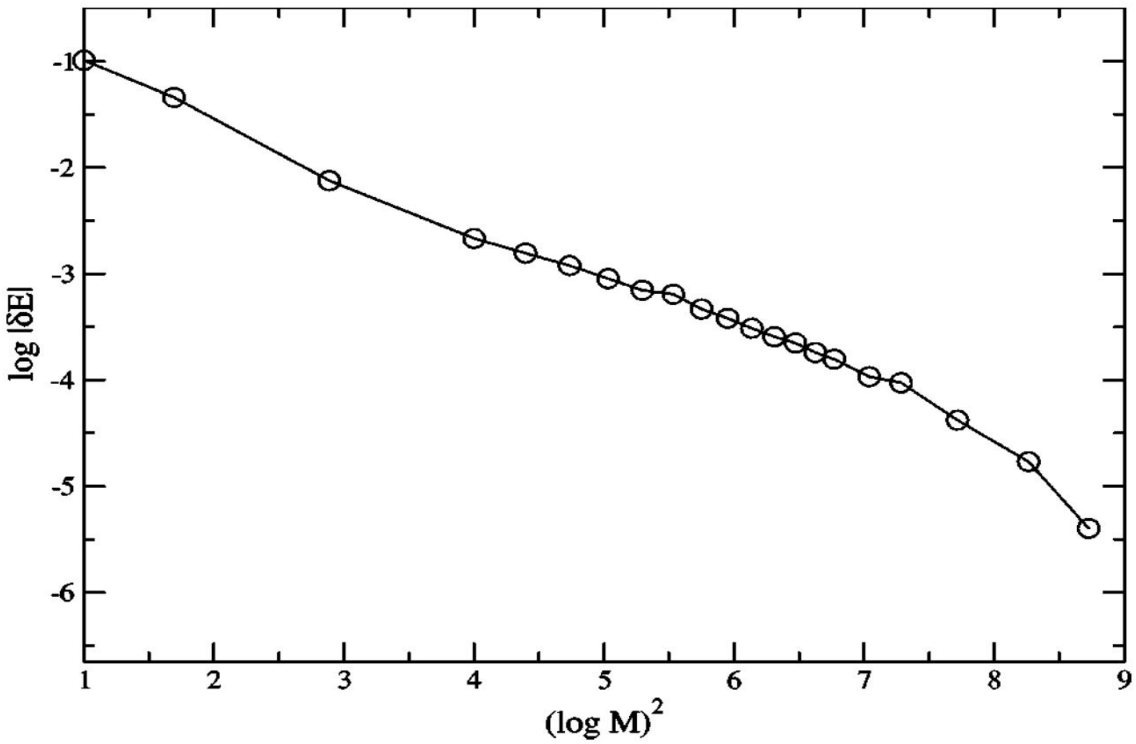

Figure 2.10: Error of DMRG calculations on the water molecule at the DZP level, as a function of M.[4]

Table 2.4: DMRG results for water in a DZP basis, with increasing the number of states M.[4]

M	E/H	δE/mH
100	-76.2545	2.1
200	-76.2559	0.71
300	-76.25632	0.32
400	-76.256477	0.157
500	-76.256540	0.094
600	-76.256592	0.042
750	-76.256617	0.017
900	-76.256624	0.004
CCSD	-76.252503	4.131
CCSD(T)	-76.255907	0.727
CCSD(TQ)	-76.256846	0.202

where the Pfaffian is a mathematical function defined from this equation. The Pfaffian of degree $2N$ with $N = 2$, for example, is written as

$$\mathrm{Pf}[\chi(i,j)] = \chi(1,2)\chi(3,4) - \chi(1,3)\chi(2,4) + \chi(1,4)\chi(2,3). \tag{2.16}$$

The AGP wavefunctions were used in QMC calculations by variational and fixed node diffusion Monte Carlo (VMC and QMC) methods [26, 27]. The VMC trial/variational wavefunction is a product of an antisymmetric part Ψ_A times a Jastrow correlation factor

$$\Psi_{VMC}(R) = \Psi_A(R)\exp[U_{corr}(r_{ij}, r_{iI}, r_{iJ})], \tag{2.17}$$

where U_{corr} depends on electron-electron, electron-ion, and electorn-electron-ion combinations of distances In the study of Refs. [27, 28, 29] with 22 variational parameters were used. In the antisymmetric part (Ψ_A), wavefunctions based on Hartree Fock and Pfaffian are used, respectively. Bajdich et al. applied these formalisms to several first row atoms and dimers (Fig. 2.11). As we can see in Fig. 2.11, they improved the description of correlation energy by the introduction of Pfaffian formalism instead of Hatree Fock. Indeed, the APG theory is known as a theory of non-interacting fermions and is variationally superior to the Hartree-Fock theory.

The quality of fermion nodes is crucial for accurate energies in the fixed node QMC. Bajdich et al. observed that the pairing correlations had an important effect on the nodal structure. Changes in the nodal manifold topology are illustrated in Fig. 2.12 for the example of an oxygen atom. As expected, the HF nodes show four nodal cells while the Pfaffian opens these artificial compartments and changes the topology to the minimal number of two nodal cells, similar to the effect of correlation observed for the Be atom.[30, 31] A comparison of Pfaffian nodes with very accurate CI nodes shows that both are qualitatively similar.

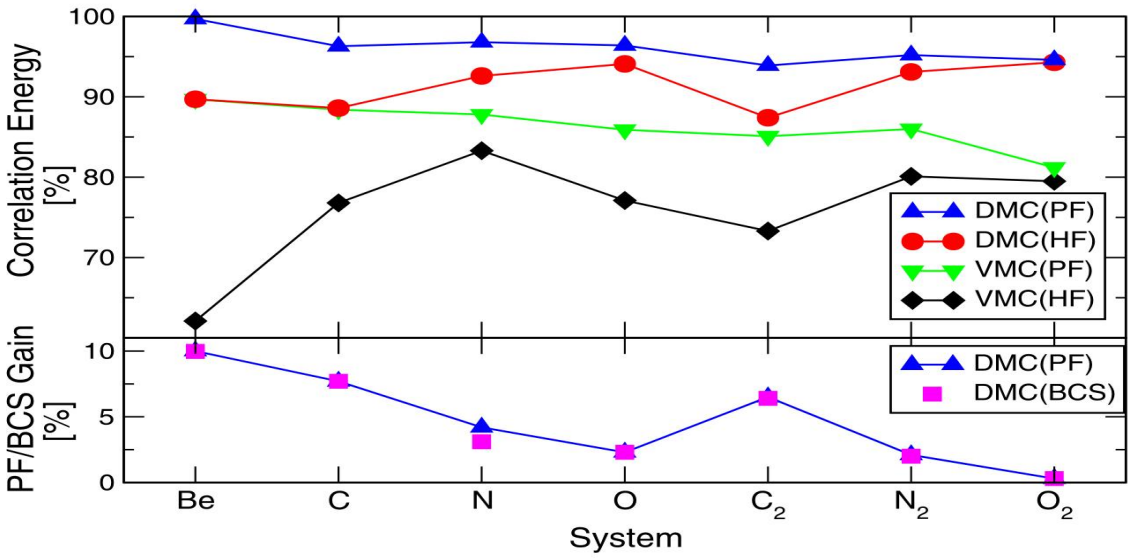

Figure 2.11: Correlation energies obtained by QMC methods with the different trial wavefunctions: VMC and fixed node DMC with HF nodes and STU Pfaffian nodes (PF). The lower plot shows the fixed node DMC correlation energy gains over HF nodes for BCS and STU Pfaffian wavefunctions. [24]

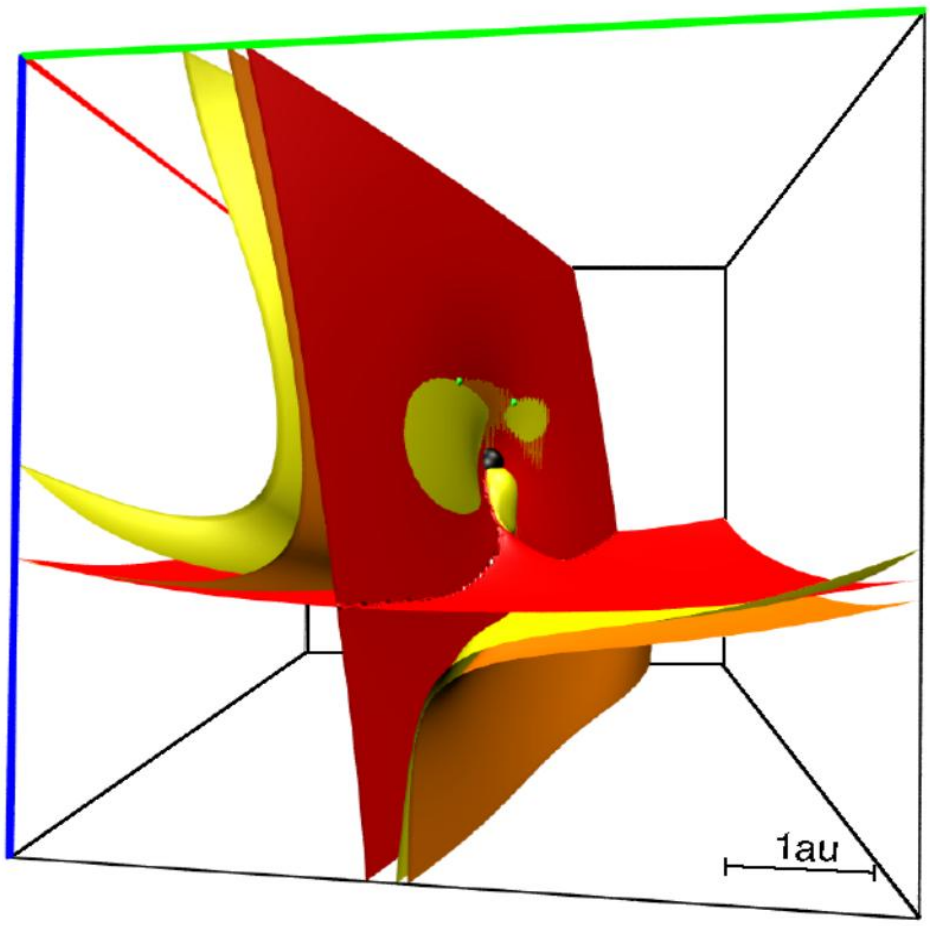

Figure 2.12: A 3D cut through the fermion node hypersurface of an oxygen atom obtained by scanning the wavefunction with a pair of spin up and spin down of electrons, both sitting at the scanning point. The remaining electrons are fixed at a given VMC snapshot position (small green spheres). The nucleus is depicted in the center of the cube by the black sphere. The three colors show nodes of: Hartree Fock (red/dark gray), STU Pfaffian nodes (orange/medium gray), and the nodes of the CI wavefunction (yellow/light gray). The CI node is very close to the exact one. The HF node clearly divides the space into four nodal cells while Pfaffian and CI wavefunctions partitioning leads to the minimal number of two nodal cells. [24]

Chapter 3

Symmetric Tensor Decomposition Description of Fermionic Many-Body Wavefunctions

Most of this Chapter has been published as:

"Symmetric Tensor Decomposition Description of Fermionic Many-Body Wave Functions"
by W. Uemura and O. Sugino, Phys. Rev. Lett. 109, 253001 (2012).

3.1 Introduction

An accurate description of the ground-state wavefunction of an interacting Fermion system is one of the central goals of modern science. The most straightforward and versatile approach to describing this wavefunction is the configuration interaction (CI), but its numerical application is greatly limited by the fact that the full-CI series consists of ${}_MC_N$ Slater determinants (SDs) when describing an N-electron system using M basis functions. To truncate this extremely long CI series without compromising on chemical accuracy, many methods have been developed, such as the multi-reference CI, which uses a part of the SDs derived from a few of the most important ones, or the complete active space (CAS) CI which uses all SDs generated from a selected set of orbitals [32]. Even so, the application has been hampered by the slow convergency of the CI series.

In this context, the many-body perturbation approaches to treat all SDs have attracted attention; these approaches include the coupled cluster (CC) theory [33][34] which is used to represent the wavefunction in terms of an SD (or a few SDs) applied with the exponential of an excitation operator. The CC theory has proven accurate for a number of molecules, although it occasionally provides qualitatively incorrect potential surfaces [35]. The density matrix renormalization group (DMRG) method [1] has also attracted attention as a variational method within the space of the matrix product state [36]. It has been extensively applied to correlated electron systems [37][38]; however, this method was originally formulated only for one-dimensional systems and its extension to three-dimensional systems is not very straightforward.

Recent tensor analyses have shown that, despite the large number, the CI coefficients may be described by a tractable number of variational parameters. For example, the full-

CI results of some molecules were accurately reproduced by the complete-graph tensor network (CGTN) state containing $\sim M^2$ variational parameters [39][40]. Tensor decomposition (TD) [41] methods such as the Tucker decomposition [42] and the canonical decomposition (CANDECOMP)/parallel factor decomposition (PARAFAC), abbreviated as CP, [43] [44] have also been applied to molecules. These methods were used to analyze the double excitation tensor $\mathcal{T}_2$ originating from the electron-electron interaction [45][46]. The results showed that the $\mathcal{T}_2$ tensor of rank 4, consisting of $\sim M^4$terms, can be described by $\sim MK$ parameters, where K denotes the length of the tensor decomposition [46]. The TD method was also suggested as being effective in greatly reducing the variational parameters required for full-CI [45].

In this context, we formulate a practical scheme to perform full-CI level calculation using a TD method. In this study, we describe the CI coefficients as a product of a symmetric tensor and the permutation tensor, and following the CP procedure we expand the former into K symmetric Kronecker product states, which are composed of vectors of dimension M. Subsequently, we calculate the second-order density matrix consisting of $\sim K^2M^4$ elements using the Vieta's formula [48] thereby performing $\sim M^2$ operations for each element. This allows us to perform the total energy calculation variationally using $\sim K^2M^6$ operations. Our test calculations for the potential surface of simple diatomic molecules and for a Hubbard cluster model with different parameters show that with increasing K, the total energy rapidly converges to the full-CI result. This shows that our symmetric tensor decomposition CI (STD-CI) scheme will greatly extend the applicability of the full-CI level calculation, provided that K increases only moderately with N, M, or the complexity of the electron correlation.

In treating the interacting indistinguishable particles, the (anti-)symmetric nature of the wavefunction plays a key role. In STD-CI, the antisymmetric nature of electrons is directly treated by explicitly introducing the permutation tensor, reducing thereby the variational degree of freedom to a power of N although it is $N!$ in the conventional CI. Moreover, the application of this scheme is not restricted to one-dimensional systems contrary to the DMRG that is based on the assumption of the matrix product state. In the rest of this paper, we provide the details of STD-CI.

3.2 The formalism of Symmetric Tensor Decomposition (STD)

We begin by describing the CI-series representation of the many-body wavefunction

$$\Psi\left(x_1 \cdots x_N\right) = \sum_{i_1 \cdots i_N = 1}^{M} A_{i_1 \cdots i_N} \psi_{i_1}\left(x_1\right) \cdots \psi_{i_N}\left(x_N\right), \tag{3.1}$$

where $x_1 \cdots x_N$ represent the space and spin coordinates of the electrons and ψ_{i_k}s are the orthonormal orbitals which are represented as a linear combination of orthonormalized basis functions as

$$\psi_i\left(x\right) = \sum_j U_{ij} \phi_j\left(x\right).$$

The antisymmetric tensor $A_{i_1\cdots i_N}$ can be described as the product of a symmetric tensor ($S_{i_1\cdots i_N}$) of rank N and dimension M and a product of $N(N-1)/2$ permutation tensors (ϵ_{ij}s) of rank 2 as

$$A_{i_1\cdots i_N} = S_{i_1\cdots i_N}\epsilon_{i_1 i_2}\epsilon_{i_1 i_3}\cdots\epsilon_{i_{N-1} i_N}. \tag{3.2}$$

Next, $S_{i_1\cdots i_N}$ is decomposed into a minimal linear combination of symmetric Kronecker product states using vectors of dimension M, $c^1_{i_k},\cdots,c^K_{i_k}$, as

$$S_{i_1\cdots i_N} = \sum_{j=1}^{K}\lambda_j c^j_{i_1}\cdots c^j_{i_N}. \tag{3.3}$$

This symmetric tensor decomposition (STD) is a symmetric version of CP, which is also a special case of the symmetric Tucker decomposition

$$S_{i_1\cdots i_N} = \sum_{j_1\cdots j_N} s_{j_1\cdots j_N}u^{j_1}_{i_1}\cdots u^{j_N}_{i_N} \tag{3.4}$$

in that the transformed tensor $s_{j_1 j_2\cdots j_N}$ is the superdiagonal λ_j in CP. The total energy is optimized by varying the vectors c^j_i and the unitary matrix U_{ij}, so that no approximation is made in our STD-CI method apart from the truncation of the series at K. It is noteworthy that each term in the STD series contains all the SDs generated from the orbitals ψ_i, although the degrees of freedom are only $MK + M(M+1)/2$ as a whole, thereby indicating that we are treating the entangled states and that the degree of entanglement is reduced with increasing K. It can be shown that the Hartree-Fock (HF) approximation corresponds to taking $K = 1$ and $c^1_{N+1} = \cdots = c^1_M = 0$; therefore, the approximation with $K = 1$ is already a natural extension of the HF approximation. When treating a weakly correlated system, an HF-like solution is obtained and on the other hand, when treating a strongly correlated system, an orbital-ordered solution is obtained, provided that a sufficiently large value of K is considered. In this manner, we can bridge the HF solution with the fully correlated state by increasing the value of K. The STD-CI will be exact when $K =_M C_N$.

3.3 Variational Procedure

Our numerical procedure begins by constructing the second-order density matrix (DM), which has the form

$$\gamma_2(x_1x_2, x_3x_4) = \sum_{i_1 i_2 i_3 i_4=1}^{M}\Gamma_{i_1 i_2 i_3 i_4}\psi^*_{i_1}(x_1)\,\psi^*_{i_2}(x_2)\,\psi_{i_3}(x_3)\,\psi_{i_4}(x_4).$$

Using (3.2) and (3.3), the DM coefficient can be rewritten as

$$\Gamma_{i_1 i_2 i_3 i_4} = \sum_{ij=1}^{K}\lambda_i\lambda_j c^{i*}_{i_1}c^{i*}_{i_2}c^j_{i_3}c^j_{i_4}\epsilon_{i_1 i_2}\epsilon_{i_3 i_4}I^{ij}_{i_1 i_2 i_3 i_4}$$

where I for each set of indices $\{iji_1i_2i_3i_4\}$ is expressed, using $a_{k_l} \equiv c^{i*}_{k_l} c^{j}_{k_l} \epsilon_{i_1k_l} \epsilon_{i_2k_l} \epsilon_{i_3k_l} \epsilon_{i_4k_l}$, as

$$I = \sum_{k_3 \cdots k_N = 1}^{M} a_{k_3} \cdots a_{k_N} \left(\epsilon_{k_3 \cdots k_N}\right)^2 . \tag{3.5}$$

Based on the fact that the permutation tensor squared is equal to 1 when all the indices are different and 0 otherwise, it can be shown using Vieta's formula that the value of I is equal to the $M-(N-2)$-th order coefficients of the polynomial $(N-2)! f_M(t)$ with $f_M(t) \equiv (t+a_1)\cdots(t+a_M)$ [48]. The coefficient can be easily obtained by using a list manipulation, where the coefficients of $f_p(t)$ with $0 \le p \le M$ are described by a row-vector of dimension p as $\boldsymbol{f}_p = (f_{p,0}, f_{p,1}, \cdots, f_{p,p-1})$ and are applied with the iterative equation, $\boldsymbol{f}_p = a_p \left(\boldsymbol{f}_{p-1}, 0\right) + \left(0, \boldsymbol{f}_{p-1}\right)$, considering $\boldsymbol{f}_0 = 1$. $\propto M^2$ operations are required to obtain the coefficient of $f_M(t)$. Therefore, the total number of operations needed to obtain all I's is $\propto K^2 M^6$. In practical coding, one may use the fact that $a_{i_k} = 0$ when i_k is equal to one of the four indices $\{i_1 i_2 i_3 i_4\}$ to achieve further efficiency.

Subsequently the parameters $c^j_{i_k}$, λ^j, and U_{ij} are varied to minimize the total energy $E_{tot} = \sum h_{i_1 i_2 i_3 i_4} \Gamma_{i_3 i_4 i_1 i_2} / \sum \Gamma_{i_1 i_2 i_1 i_2}$ with

$$\begin{aligned} h_{i_1 i_2 i_3 i_4} &= \int dx_1 dx_2 \psi^*_{i_1}(x_1) \psi^*_{i_2}(x_2) \left[N \left(-\frac{1}{2} \boldsymbol{\nabla}^2_1 + v_{ext}(\boldsymbol{r}_1) \right) + \frac{N(N+1)}{2} \frac{1}{|\boldsymbol{r}_1 - \boldsymbol{r}_2|} \right] \\ &\times \psi_{i_3}(x_1) \psi_{i_4}(x_2) , \end{aligned} \tag{3.6}$$

where v_{ext} denotes the external potential. In the variation, we require derivatives of $I^{ij}_{i_1 i_2 i_3 i_4}$ with respect to a_{i_k} for those i_k not in $\{i_1 i_2 i_3 i_4\}$. To obtain the derivatives, we need to differentiate $f_M(t)$ by a_{i_k} and obtain its $M-(N-1)$-th coefficient. When this is done simply using the list manipulation, $\propto K^2 M^7$ operations are required for each i_k; however, the number of operations can be reduced when using $f_M(t)/(t+a_{i_k})$ for the differentiation. When the series $(t+a_{i_k})^{-1} = \sum_{m=0}^{\infty} a_{i_k}^{-m-1} (-t)^m$ is multiplied with $f_M(t)$, the $M-(N-1)$-th coefficient can be obtained as

$$-\sum_{s=0}^{M-(N-1)} (-a_{i_k})^{s-1-M+(N-1)} f_{M,s},$$

thereby requiring $\propto M$ operations for each k. Therefore, $\sim K^2 M^6$ operations are required to obtain all the derivatives of $I^{ij}_{i_1 i_2 i_3 i_4}$. By applying the same technique to the expression $f(t)/(t+a_i)(t+a_j)$, the second derivatives are similarly obtained with $\propto K^2 M^6$ operations. It should be noted that the calculation of the derivatives is the rate-determining step in our calculation.

In a manner similar to HF [50],[51], STD-CI can be applied to a crystalline solid by taking a linear combination of the atomic orbitals χ_i as

$$\phi_{ik}(r) = \sum_{\tau} e^{ik \cdot R_\tau} \chi_i (r - R_\tau) ,$$

where k and R_τ denote the reciprocal vector in the Brillouin zone and the nuclear coordinate, respectively. Thus, M should be read as the number of k values multiplied by the number of basis functions.

3.4 Numerical Results

To assess the efficiency of STD-CI, we investigate how many terms in Eq.(3.3) are required to achieve convergence in E_{tot}. This investigation is carried out for simple diatomic molecules (H_2, He_2, and LiH) and a four-site Hubbard model. Relativistic effects are neglected and only the spin unpolarized state is calculated by using the same number of orbitals with an α and β spin. In testing the convergence, the calculated results are compared with the full CI calculation performed using the same basis functions. In our calculations, the Newton-Raphson method is used to variationally determine the parameters.

H_2 is the simplest molecule where the molecular orbital picture, valid near the equilibrium bond length, is switched to the Heitler-London picture, as the interatomic distance increases to infinity. The calculation with the STO-3G basis set shows that $K = 1$ reproduces the full CI potential curve within an error of 0.01 Ha error, while the error is less than 0.01 mHa when $K = 2$ (Fig. 3.1). The molecule He_2 is weakly bound the dispersion forces and the test is more stringent in this case. The calculation with the 6-311G basis set shows that $K = 3$ is sufficient to reproduce the full CI result within an error of 0.01 mHa, while $K = 2$ is already sufficient to obtain the binding energy within the same accuracy although the absolute value of E_{tot} is always larger by 0.1 mHa (Fig. 3.2). The binding energy is about three times larger than the accurate quantum chemical calculation[52] and the experimental results [53], which is presumably due to the insufficient number of basis functions; obtaining an accurate value of the binding energy is beyond the scope of our comparative study, and this must be the consideration of future studies. LiH is a typical hetero-nuclear diatomic molecule. The 4-31G calculation for this case shows that $K = 1$ nearly sufficiently reproduces the full CI result while the HF calculation significantly underestimates the binding energy (Fig. 3.3). The final test is the application of our idea to the four-site Hubbard model in the tetrahedron structure under the half-filled condition. As the Hubbard U over the transfer t increases, larger K values are required; however, $K = 6$ is found sufficient even in the large U/t limit (Fig. 3.4).

The computational time theoretically scales as K^2M^6. We tested the time scaling with our numerical code to find that CPU time indeed scales as $K^{1.97}M^{5.97}$ on average (Figs. 3.5,3.6). Because the operations involved in the calculation can be performed independently, this method is suitable for massively parallel computers.

Fig. 3.7 shows the dependence of the energy on the orbital number M. In this result, we are treating LiH molecule with the atomic distance $R = 3.0$. In STD-CI, we can change the number of orbitals M between the number of electrons N and the number of basis set B. In this system, $N = 4$ and $B = 22$. When $M = N$, the result of STD-CI is equivalent to that of Hatree-Fock. As we increase M from N, the resulting energy quickly approaches to the result of $M = B$. This means that we do not have to set M equal to B. With smaller value of M, the total calculation cost will decrease. We interpret on this result that M is enough when set to $M = 2N$ to reproduce sufficient accuracy of the energy.

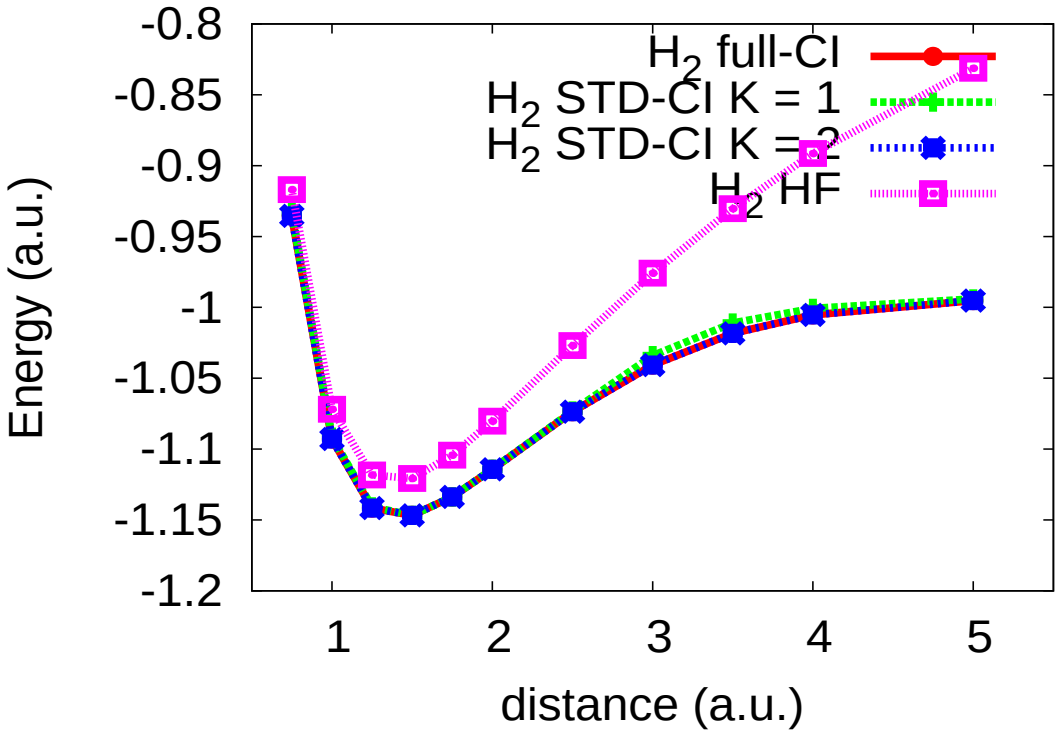

Figure 3.1: Potential curve of H_2 molecules for full-CI (solid line with circle), STD-CI with $K = 1$ (broken line with cross) and $K = 2$ (broken line with asterisk), and HF (dotted line with rectangle).

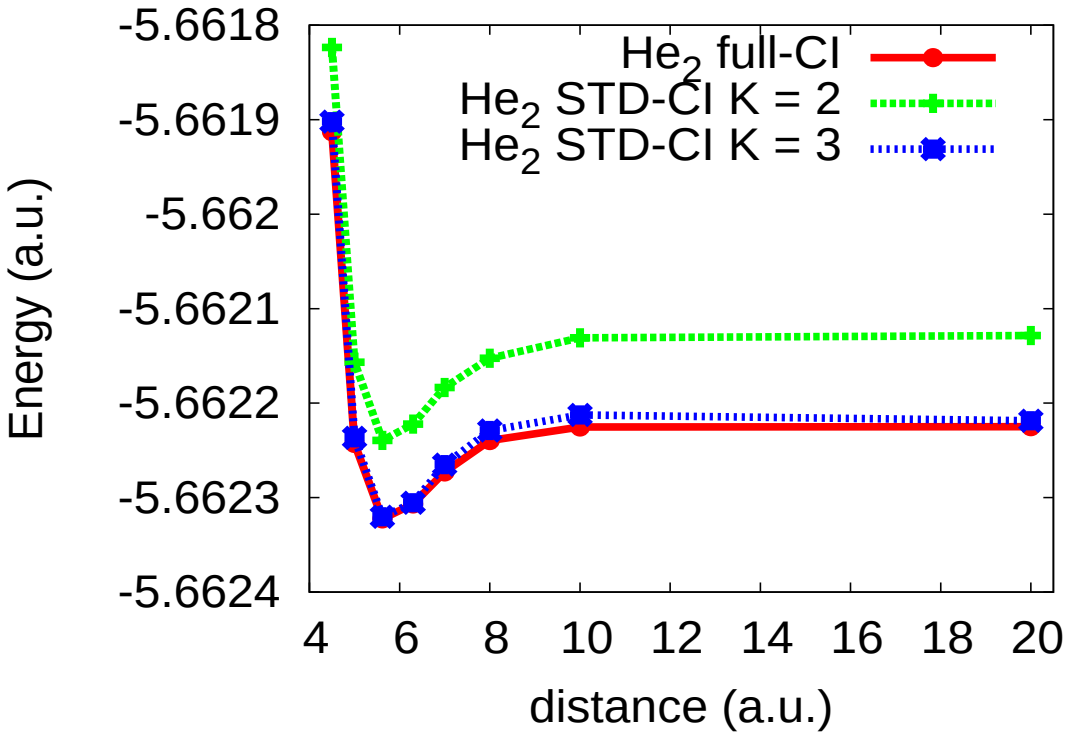

Figure 3.2: Potential curve of He_2 molecules for full-CI (solid line with circle) and STD-CI with $K = 2$ (broken line with cross) and $K = 3$ (broken line with asterisk).

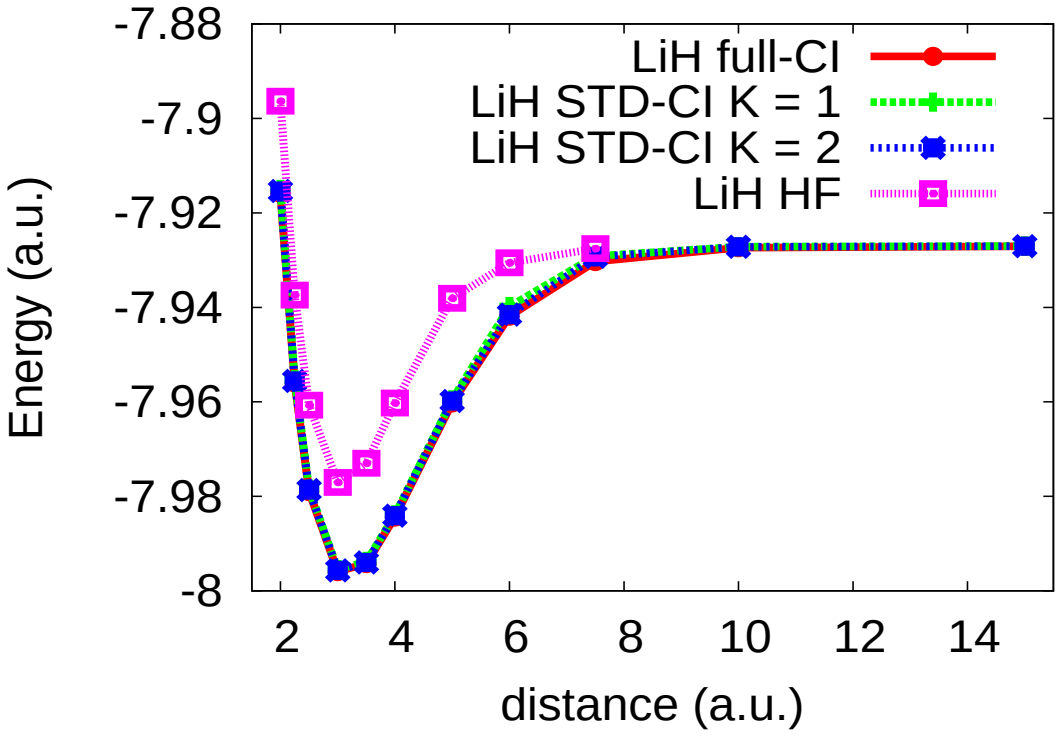

Figure 3.3: Potential curve of LiH molecules for full-CI (solid line with circle), STD-CI with $K = 1$ (broken line with cross) and $K = 2$ (broken line with asterisk), and HF (dotted line with rectangle).

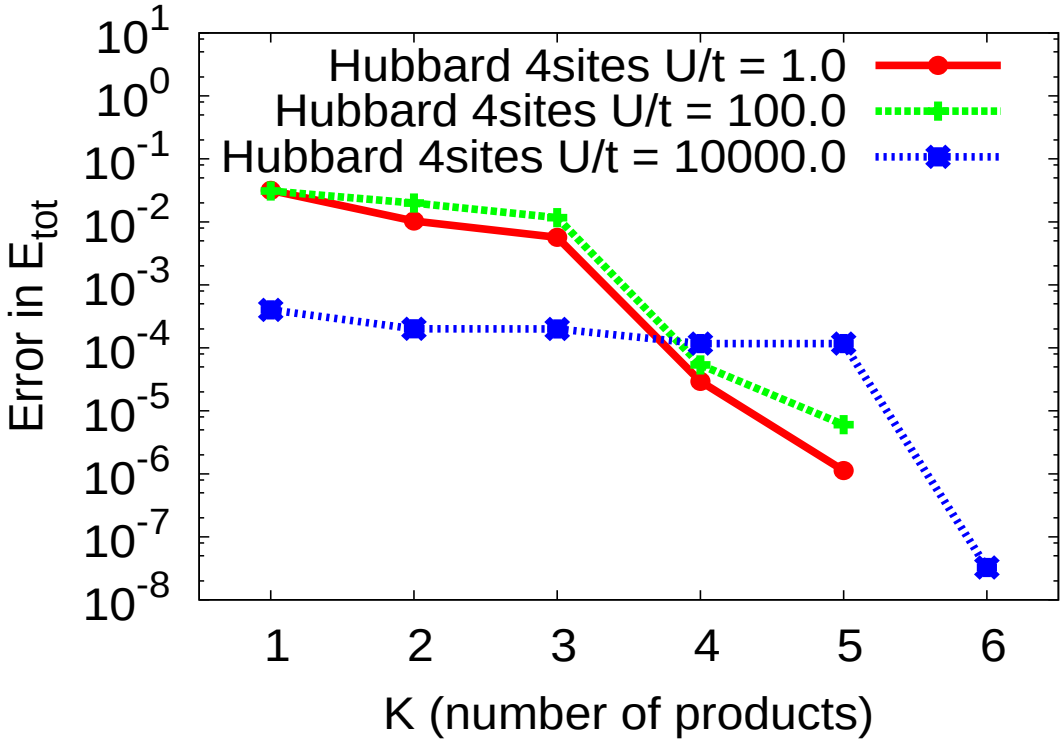

Figure 3.4: Error in E_{tot} for the four-site Hubbard model for various parameters $U/t = 1$ (solid line with circle), $U/t = 100$ (dotted line with cross), and $U/t = 10000$ (dotted line with asterisk).

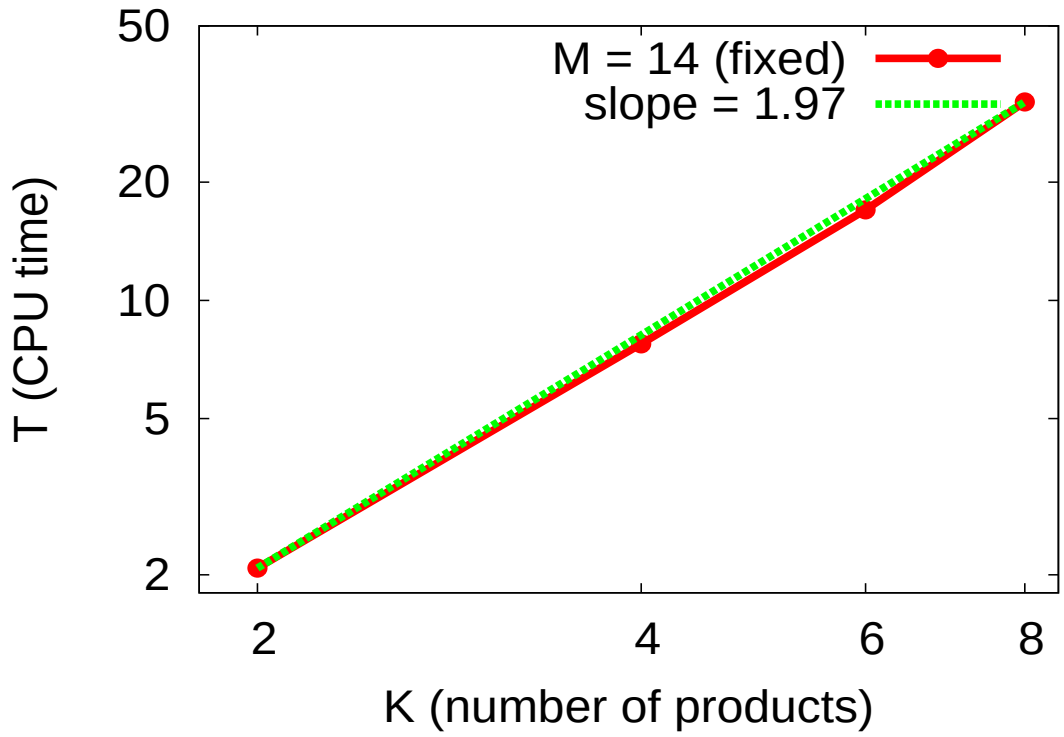

Figure 3.5: Total CPU time (T) versus K. The solid line with circle indicates result after measurement for one iteration step and the broken line indicates that after fitting to $T = aK^b$. b is obtained as 1.97.

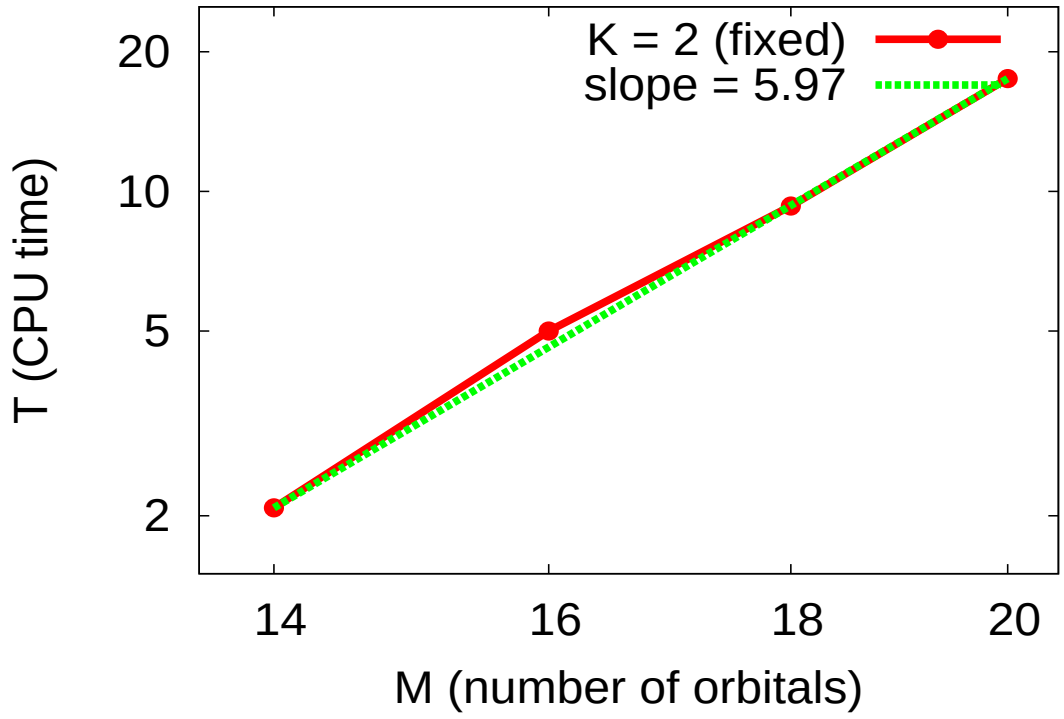

Figure 3.6: Total CPU time (T) versus M. The solid line with circle indicates result after measurement for one iteration step and the broken line indicates that after fitting to $T = aM^b$. b is 5.97 after the fitting.

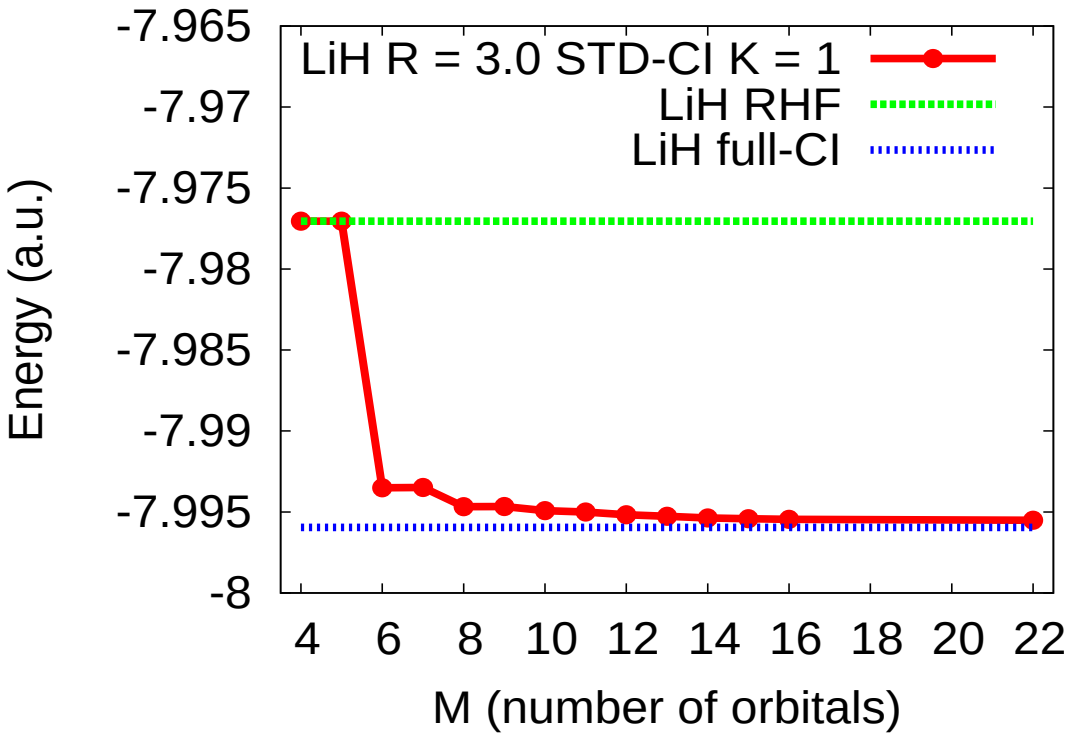

Figure 3.7: Total energy of LiH as a function of the orbital number M. Results of Hatree-Fock and full CI are also shown in the figure.

3.5 Conclusion

We formulated a practical scheme to perform the full-CI level calculation using the STD method. In the STD-CI method, we expand the CI coefficients as the product of a symmetric tensor and the permutation tensor, and we further expand the symmetric tensor into Kronecker product states composed of vectors of dimension M. By varying the vectors and the unitary transformation matrix U_{ij}, the total energy is minimized using the second-order density matrix technique. The STD-CI method, which involves taking the length of the series K as the only input parameter, allows us to perform a full-CI level calculation rigorously using $KM + M\left(M+1\right)/2$ variational parameters and $\sim K^2M^6$ operations. By applying the scheme to the potential curve of small diatomic molecules such as H_2, He_2, and LiH, and the four-site Hubbard model for various parameters, we found that a very small K value is required to reproduce the full-CI results within milli-Hartree accuracy. If K increases moderately with N, M, or the degree of correlation, the scheme will greatly extend the applicability of the full-CI level calculation. We believe that application of the scheme to a crystalline solid and the use of the scheme as a building block of the fragment molecular orbital (FMO) scheme can be of high significance[54].

Acknowledgement

The authors thank Prof. Y. Mochizuki (Rikkyo Univ.) and M. Nakata (RIKEN) for their valuable discussions.

Chapter 4

Extended Symmetric Tensor Decomposition in Fermionic Wavefunctions

4.1 Introduction

Symmetric Tensor Decompostion Configuration Interaction (STD-CI) sometime requires large value for the rank of the tensor decomposition K, especially for more strongly correlated systems such as H_2O. In our computer program, the numerical calculation tends to be less stable as the rank is increased. It is also generally known that the Symmetric Tensor Decomposition, or the Canonical Decomposition (CP) becomes numerically tough when the number of the terms (K) becomes larger, say larger than 10. In Extended Symmetric Tensor Decomposition (ESTD), we use K set of general matrices for the transformation of the base to the orbital though we have used only one unitary matrix in STD-CI. In ESTD-CI, we assume that the total number of electrons (N) is even.

4.2 The formalism of Extended Symmetric Tensor Decomposition (ESTD)

In STD-CI, we have used the algorithm where the permutation tensor of rank N is decomposed into pieces, i.e., the product of the permutation tensors of rank 2. In ESTD, we use a different decomposition that leads eventually to an improvement of the theory. There are representations of the permutation tensor based on geminals. The representation for small rank is

$$\epsilon_{i_1 i_2 i_3} = \epsilon_{i_1 i_2} + \epsilon_{i_2 i_3} + \epsilon_{i_3 i_1}, \tag{4.1}$$

$$\epsilon_{i_1 i_2 i_3 i_4} = \epsilon_{i_1 i_2}\epsilon_{i_3 i_4} + \epsilon_{i_1 i_3}\epsilon_{i_4 i_2} + \epsilon_{i_1 i_4}\epsilon_{i_2 i_3}, \tag{4.2}$$

which is generally written as

$$\epsilon_{i_1 \cdots i_N} = \hat{A}(\epsilon_{i_1 i_2}\epsilon_{i_3 i_4} \cdots \epsilon_{i_{N-1} i_N}) \text{ for even } N. \tag{4.3}$$

Here $\hat{A}$ is the antisymmetrizer that sums up all the terms obtained by permutating all the indices $i_1, i_2, \ldots, i_N$, except for exchange within the pair (the two appearing as the

subscript of the same ϵ matrix) and exchange of the pairs, such as $i_1, i_2, i_3, i_4 \to i_3, i_4, i_1, i_2$. N is the number of electrons. In the summation, each term is assigned a sign according to the evenness/oddness of the permutation.

In the ESTD theory, the wavefuntion is extended as is written as

$$A_{i_1 \cdots i_N} = \sum_{k_1 \cdots k_N} \epsilon_{k_1 \cdots k_N} \alpha_{k_1 i_1} \cdots \alpha_{k_N i_N}. \tag{4.4}$$

More generally

$$A_{i_1 \cdots i_N} = \sum_{k=1}^{K} c_k \sum_{k_1 \cdots k_N} \epsilon_{k_1 \cdots k_N} \alpha^k_{k_1 i_1} \cdots \alpha^k_{k_N i_N}, \tag{4.5}$$

where tensor A is the antisymmetric tensor that corresponds to the total wavefunction of electrons. α^is are general matrices as parameters from which the total wavefunction is defined. In the STD-CI wavefunciton, the matrices are restricted to be unitary and are independent of k, but in ESTD different set of the matrix are used for different k. In this respect the variational degrees of freedom are extended.

To evaluate the total energy or expectation value of an observable, it is convenient to introduce the generating function which will be called wavefunction norm n,

$$n = \sum_{i_1 \cdots i_N j_1 \cdots j_N} \epsilon_{i_1 \cdots i_N} \epsilon_{j_1 \cdots j_N} a_{i_1 j_1} \cdots a_{i_N j_N}, \tag{4.6}$$

where

$$a \equiv \alpha^t \alpha, \tag{4.7}$$

more generally

$$a^{xy} \equiv \alpha^{x\,t} \alpha^y \tag{4.8}$$

and

$$n^{xy} = \sum_{i_1 \cdots i_N j_1 \cdots j_N} \epsilon_{i_1 \cdots i_N} \epsilon_{j_1 \cdots j_N} a^{xy}_{i_1 j_1} \cdots a^{xy}_{i_N j_N}. \tag{4.9}$$

for x and y in $\{1, \ldots, K\}$. The role of the norm is that expectation values can be easily obtained by differentiating the norm with respect to the variational parameter, as will be shown below. It is worth emphasizing that ESTD is easily adapted to non-orthogonal basis functions $\{\phi_i\}$, because we just need to modify the definition as

$$a^{xy} \equiv \alpha^x u\, {}^t \alpha^y \tag{4.10}$$

where the overlap matrix is given by

$$u_{ij} \equiv \langle \phi_i \,|\, \phi_j \rangle \,. \tag{4.11}$$

The wavefunction norm for $N = 4$ is

$$n = 3(\mathrm{tr}\, A)^2 - 6(\mathrm{tr}\, A^2), \tag{4.12}$$

and that for $N = 6$ is

$$n = 15(\mathrm{tr}\, A)^3 - 90(\mathrm{tr}\, A)(\mathrm{tr}\, A^2) + 120(\mathrm{tr}\, A^3), \tag{4.13}$$

where

$$A \equiv a\epsilon^t a^t \epsilon. \tag{4.14}$$

The general result is

$$\begin{aligned} n &= N! \exp(\frac{1}{2}\mathrm{tr}\log(1+At))|_{t^{N/2}} && (4.15)\\ &\equiv N!\,\mathrm{pf}(1+At)|_{t^{N/2}}. && (4.16)\end{aligned}$$

Here the symbol $|_{t^{N/2}}$ indicates that we take the $N/2$-th order term of the whole expression with respect to t. This is the key result of this work. Because of the very simple form for the norm, we can dramatically reduce the number of operations required for the variational calculation. We will provide a sequence of proofs for this main result in the following sentences.

Theorem 1 *(Decomposition of the permutation tensor)*

$$\begin{aligned}\epsilon_{i_1 \ldots i_N} &= \frac{1}{2^{N/2}\left(\frac{N}{2}\right)!}\sum_{\sigma\in S_N}\mathrm{sgn}\,(\sigma)\prod_{n=1}^{N/2}\epsilon_{i_{\sigma(2n-1)}i_{\sigma(2n)}}\\ &= \sum_{\sigma\in S_N^*}\mathrm{sgn}\,(\sigma)\prod_{n=1}^{N/2}\epsilon_{i_{\sigma(2n-1)}i_{\sigma(2n)}}\\ &= \hat{A}\left(\epsilon_{i_1 i_2}\epsilon_{i_3 i_4}\cdots\epsilon_{i_{N-1}i_N}\right),\end{aligned}$$

where S_N is the permutation and S_N^* is the subset of S_N such that $S_N = S_N^* \otimes S_N^0$ with $S_N^0 \equiv$ $\{$exchange between $2n-1$ and $2n$, and exchange between $(2n-1, 2n)$ and $(2m-1, 2m)\}$.

Proof is straightforward and will not be shown here. With this theorem the norm is reduced as

$$\rho = \sum_{i_1,\ldots,i_N}\sum_{j_1,\ldots,j_N}\sum_{\sigma\in S_N^*}\mathrm{sgn}\,(\sigma)\,\epsilon_{i_1,\ldots,i_N}\epsilon_{j_{\sigma(1)}j_{\sigma(2)}}\cdots\epsilon_{j_{\sigma(N-1)}j_{\sigma(N)}}a_{i_1 j_1}\cdots a_{i_N j_N},$$

and replacing the indices as $k \longleftrightarrow \sigma(k)$ yields

$$\rho = \sum_{i_1,\ldots,i_N}\sum_{j_1,\ldots,j_N}\sum_{\sigma\in S_N^*}\mathrm{sgn}\,(\sigma)\,\epsilon_{i_{\sigma(1)},\ldots,i_{\sigma(N)}}\epsilon_{j_1 j_2}\cdots\epsilon_{j_{N-1}j_N}a_{i_1 j_1}\cdots a_{i_N j_N}.$$

Since the sum is invariant with respect to a permutation σ,

$$\rho = \sum_{i_1,\ldots,i_N}\sum_{j_1,\ldots,j_N}\frac{(N)!}{2^{N/2}\left(\frac{N}{2}\right)!}\epsilon_{i_1,\ldots,i_N}\epsilon_{j_1 j_2}\cdots\epsilon_{j_{N-1}j_N}a_{i_1 j_1}\cdots a_{i_N j_N}.$$

Applying the theorem again, we get

$$\begin{aligned}\rho &= \sum_{i_1,\ldots,i_N}\sum_{j_1,\ldots,j_N}\frac{(N)!}{2^{N/2}\left(\frac{N}{2}\right)!}\frac{1}{2^{N/2}\left(\frac{N}{2}\right)!}\sum_{\sigma\in S_N}\mathrm{sgn}\,(\sigma)\,\epsilon_{i_{\sigma(1)}i_{\sigma(2)}}\cdots\epsilon_{i_{\sigma(N-1)}i_{\sigma(N)}}\epsilon_{j_1 j_2}\cdots\epsilon_{j_{N-1}j_N}a_{i_1 j_1}\cdots a_{i_N j_N}\\ &= \sum_{i_1,\ldots,i_N}\sum_{j_1,\ldots,j_N}\frac{(N)!}{2^{N/2}\left(\frac{N}{2}\right)!}\sum_{\sigma\in S_N^*}\mathrm{sgn}\,(\sigma)\,\epsilon_{i_{\sigma(1)}i_{\sigma(2)}}\cdots\epsilon_{i_{\sigma(N-1)}i_{\sigma(N)}}\epsilon_{j_1 j_2}\cdots\epsilon_{j_{N-1}j_N}a_{i_1 j_1}\cdots a_{i_N j_N}.\end{aligned}$$

Now we define the sequence that starts from, say i_1, and connects indices as $i_1 \to j_1$using the index of a, $j_1 \to j_2$ using that of ϵ, using $j_2 \to i_2$ using that of a, and $i_2 \to i_{\bar{2}}$ using that of ϵ, where $\bar{2}$ indicates the counterpart of the index 2 in an ϵ matrix such that $\epsilon_{i_2 i_{\bar{2}}}$. The sequence returns to the starting point and make a cycle. When the matrices are arranged along the sequence, we get

$$a_{i_1 j_1} \epsilon_{j_1 j_2}{}^t a_{j_2 i_2}{}^t \epsilon_{i_2 i_{\bar{2}}} \cdots {}^t \epsilon_{i_{\bar{1}} i_1},$$

which yields a trace

$$\mathrm{tr}\left[\left(a\epsilon^t a^t \epsilon\right)^q\right].$$

Using the traces of various lengths formed this way, the norm can be rewritten. Note that the signature of the permutation corresponds to $(-1)^{q+1}$. We will now obtain the coefficient for such cycles expansion.

First, let us count how many (L_N) cycles of full length, N, will appear. When the number of smaller cycles is known as L_{N-2}, we can obtain L_N because we can break one of the bonds connecting two i's and connect the broken bonds to the sites $N-1$ and N to produce different full cycles. Since the number of ways to break the bonds is $(N/2-1)\, L_{N-2}$ and two ways for the connection, we find the relation

$$L_N = (N-2)\, L_{N-2},$$

and

$$L_N = 2^{N/2-1}\, (N/2-1)!$$

using the fact that $L_2 = 1$.

Second, we can now count the number of terms consisting of smaller cycles. When, for example, the cycles contain one of length $N-2$ and the other of length 2, the number is

$${}_{N/2}C_1 L_{N-2} L_2,$$

and when the cycles contain one of length $N-4$ and two of length 2,

$${}_{N/2}C_2 L_{N-4} \left(L_2\right)^2.$$

When $N = 8$ and counting the terms of two cyles of length 4, the number is

$$\frac{{}_4C_2}{2} \left(L_4\right)^2,$$

where the factor $1/2$ comes from permutation of the two equivalent cycles.

This way we get, taking into account of the signatures,

$$\begin{aligned}
\rho = (N)! & \frac{(-1)^{N/2+1}\, \mathrm{tr}\left[\left(a\epsilon^t a^t \epsilon\right)^{N/2}\right]}{N} \\
& + (N)! \frac{(-1)^{N/2}\, \mathrm{tr}\left[\left(a\epsilon^t a^t \epsilon\right)^{N/2-1}\right]}{2\,(N/2-1)} \frac{\mathrm{tr}\left[\left(a\epsilon^t a^t \epsilon\right)\right]}{2} \\
& + (N)! \frac{(-1)^{N/2-1}\, \mathrm{tr}\left[\left(a\epsilon^t a^t \epsilon\right)^{N/2-2}\right]}{2\,(N/2-2)} \left\{\frac{\mathrm{tr}\left[\left(a\epsilon^t a^t \epsilon\right)\right]}{2}\right\}^2 \frac{1}{2} \\
& + \cdots.
\end{aligned}$$

This result may be generalized as

$$\rho = (N)! \sum_{k_1 k_2 \cdots}^{k_1+2k_2+\cdots=N/2} \prod_q \frac{1}{k_q!} \left(\frac{(-1)^{q+1} \operatorname{tr}\left[(a\epsilon^t a^t \epsilon)^q\right]}{2q} \right)^{k_q} \tag{4.17}$$

In the following theorem we show that the coefficients can be compactly represented as the polynomial coefficients of a Pfaffian.

Theorem 2 *(Norm and Pfaffian): The norm ρ, defined using general matrix a by*

$$\rho \equiv \sum_{i_1,\ldots,i_N} \sum_{j_1,\ldots,j_N} \epsilon_{i_1 \ldots i_N} \epsilon_{j_1 \ldots j_N} a_{i_1 j_1} \cdots a_{i_N j_N},$$

is given by $N/2$-th degree coefficient of the Fredholm Pfaffian as

$$\rho = (N)! \operatorname{pf}\left(1 + (a\epsilon)^t (\epsilon a)\, t\right)\big|_{t^{N/2}},$$

where the Fredholm Pfaffian is defined for a general matrix A in terms of Taylor series of the following:

$$\operatorname{pf}(1 + At) \equiv \exp\left[\frac{1}{2}\operatorname{tr}\left[\log(1 + At)\right]\right].$$

Proof. Taking Taylor expansion, we have

$$\begin{aligned}
&\operatorname{pf}\left(1 + (a\epsilon)^t (\epsilon a)\, t\right) \\
&= \sum_{n=0} \frac{1}{(n)!} \left(\frac{1}{2}\operatorname{tr}\left(\sum_{p=1} \frac{(-1)^{p+1}}{p} \left(a\epsilon^t a^t \epsilon\right)^p t^p \right) \right)^n \\
&= \sum_{n=0} \sum_{k_1 k_2 \cdots}^{k_1+2k_2+\cdots=n} \prod_{p=1} \frac{(-1)^{(p+1)k_p} \left(\operatorname{tr}\left[(a\epsilon^t a^t \epsilon)^p\right]\right)^{k_p}}{(k_p!)\,(2p)^{k_p}} t^n,
\end{aligned}$$

where the multinomial theorem has been used. The summation under the restriction, $\sum_p p k_p = n$, corresponds to partitioning $2n$ into k_p groups of size $2p$. In the partitioning, there are $k_p!\,(2p)^{k_p}$ equivalent ones corresponding to exchange within the group, $(2p)^{k_p}$, and that between the groups, $k_p!$. By comparing with Eq. (4.17), the coefficients are equal to that equation when $n = N/2$. This proves the theorem. ■

The matrix A is a product of 2 skew symmetric matrices because in (4.14), both $a\epsilon^t a$ and ${}^t\epsilon$ are skew symmetric matrices. Therefore A has evenly degenerate eigenvalues[55]. When the eigenvalues of A are $\lambda_1, \lambda_1, \ldots, \lambda_{M/2}, \lambda_{M/2}$,

$$\begin{aligned}
n &= N!\operatorname{pf}(1 + At)|_{t^{N/2}} \\
&= N!\left(\det(1 + At)\right)^{1/2}|_{t^{N/2}} \\
&= N!\sqrt{(1 + \lambda_1 t)^2 \cdots (1 + \lambda_{M/2} t)^2}|_{t^{N/2}} \\
&= N!\left((1 + \lambda_1 t) \cdots (1 + \lambda_{M/2} t)\right)|_{t^{N/2}}.
\end{aligned} \tag{4.18}$$

Therefore the polynomial of (4.15) can be expressed as an $M/2$-th order polynomial of t. For this reason we named this polynomial as Pfaffian, considering the fact that this polynomial is a square root of the Fredholm determinant $\det(1 + At)$.

As we do in STD-CI, we describe the total energy using the second-order density matrix, which is obtained in ESTD-CI from the derivatives of the norm. The second order reduced density matrix Γ can be given by taking the second derivative for n.

$$\begin{aligned}
&\frac{\partial}{\partial a_{k_1l_1}}\frac{\partial}{\partial a_{k_2l_2}}\sum_{i_1\cdots i_N j_1\cdots j_N} a_{i_1j_1}\cdots a_{i_Nj_N}\epsilon_{i_1\cdots i_N}\epsilon_{j_1\cdots j_N} \\
= \;& N(N-1)\sum_{i_1\cdots i_N j_1\cdots j_N} \delta_{i_1k_1}\delta_{j_1l_1}\delta_{i_2k_2}\delta_{j_2l_2}a_{i_3j_3}\cdots a_{i_Nj_N}\epsilon_{i_1\cdots i_N}\epsilon_{j_1\cdots j_N} \\
= \;& N(N-1)\sum_{i_3\cdots i_N j_3\cdots j_N} a_{i_3j_3}\cdots a_{i_Nj_N}\epsilon_{k_1k_2i_3\cdots i_N}\epsilon_{l_1l_2j_3\cdots j_N}, \qquad (4.19)
\end{aligned}$$

$$\Gamma_{i_1j_1i_2j_2} = \sum_{k_1l_1k_2l_2}\alpha_{k_1i_1}\alpha_{l_1j_1}\alpha_{k_2i_2}\alpha_{l_2j_2}\frac{\partial}{\partial a_{k_1l_1}}\frac{\partial}{\partial a_{k_2l_2}}n. \qquad (4.20)$$

Before providing detailed equations for the density matrices, we state relationship of ESTD to AGP. The wavefunction of ESTD can be regarded as a linear combination of Antisymmetrized Geminal Power (AGP) wavefunctions[56][57].

$$\begin{aligned}
A_{i_1\cdots i_N} &= \sum_{k_1\cdots k_N}\hat{A}(\epsilon_{k_1k_2}\epsilon_{k_3k_4}\cdots\epsilon_{k_{N-1}k_N})\alpha_{k_1i_1}\cdots\alpha_{k_Ni_N} \\
&= \hat{A}(\gamma_{i_1i_2}\gamma_{i_3i_4}\cdots\gamma_{i_{N-1}i_N}), \qquad (4.21)
\end{aligned}$$

where

$$\gamma_{i_1i_2} \equiv \sum_{k_1k_2}\epsilon_{k_1k_2}\alpha_{k_1i_1}\alpha_{k_2i_2} \qquad (4.22)$$

is an antisymmetric geminal. For two geminals γ^x and γ^y, the resulting norm (4.6) with two wavefunctions from these geminals is represented as

$$n^{xy} = N!\,\mathrm{pf}(1-\gamma^x\gamma^y t)|_{t^{N/2}}. \qquad (4.23)$$

The AGP theory is for non-interacting fermions and is an extension of the Hartree-Fock theory. To treat interacting fermions, we need to introduce correlation between geminals. Although the correlation factor is multiplied in the variational MC scheme, we use different way, that is, we take linear combination of AGP. In this sense ESTD is a theory for interacting geminals.

4.3 The energy and the first derivatives in ESTD-CI

The energy can be obtained from the second order reduced density matrix. The energy can be calculated in $O(M^5K^2)$ steps. In this subsection we provide the expression for the energy and, with that, we will show how the number of operations scales with the system size.

Using the second derivative of the norm, the energy is written as

$$
\begin{aligned}
E &= \sum_{k_1 l_1 k_2 l_2} H^a_{k_1 l_1 k_2 l_2} \frac{1}{2} \frac{\partial}{\partial a_{k_1 l_1}} \frac{\partial}{\partial a_{k_2 l_2}} \mathrm{pf}(1+At)|_{t^{N/2}} \\
&= \sum_{k_1 l_1 k_2 l_2} H^a_{k_1 l_1 k_2 l_2} \frac{1}{2} \mathrm{pf}(1+At) \\
&\quad (\frac{1}{2}\mathrm{tr}((1+At)^{-1} \frac{\partial^2}{\partial a_{k_1 l_1} \partial a_{k_2 l_2}} At \\
&- \frac{1}{2}\mathrm{tr}((1+At)^{-1} \frac{\partial A}{\partial a_{k_1 l_1}} (1+At)^{-1} \frac{\partial A}{\partial a_{k_2 l_2}}) t^2 \\
&+ \frac{1}{4}\mathrm{tr}((1+At)^{-1} \frac{\partial A}{\partial a_{k_1 l_1}}) \mathrm{tr}((1+At)^{-1} \frac{\partial A}{\partial a_{k_2 l_2}}) t^2)|_{t^{N/2}} \\
&= \sum_{k_1 l_1 k_2 l_2} H^a_{k_1 l_1 k_2 l_2} \frac{1}{2} \mathrm{pf}(1+At) \\
&\quad (\frac{1}{2}((^t\epsilon(1+At)^{-1})_{k_2 k_1} \epsilon_{l_1 l_2} + (^t\epsilon(1+At)^{-1})_{k_1 k_2} \epsilon_{l_2 l_1}) t \\
&- \frac{1}{2}((\epsilon^t a^t \epsilon (1+At)^{-1})_{l_2 k_1} (\epsilon^t a^t \epsilon (1+At)^{-1})_{l_1 k_2} \\
&+ (^t\epsilon(1+At)^{-1})_{k_2 k_1} (\epsilon^t a^t \epsilon (1+At)^{-1} a\epsilon)_{l_1 l_2} \\
&+ (\epsilon^t a^t \epsilon (1+At)^{-1} a\epsilon)_{l_2 l_1} (^t\epsilon(1+At)^{-1})_{k_1 k_2} \\
&+ (^t\epsilon(1+At)^{-1} a\epsilon)_{k_2 l_1} (^t\epsilon(1+At)^{-1} a\epsilon)_{k_1 l_2}) t^2 \\
&+ \frac{1}{4}((\epsilon^t a^t \epsilon (1+At)^{-1})_{l_1 k_1} (\epsilon^t a^t \epsilon (1+At)^{-1})_{l_2 k_2} \\
&+ (\epsilon^t a^t \epsilon (1+At)^{-1})_{l_1 k_1} (^t\epsilon(1+At)^{-1} a\epsilon)_{k_2 l_2} \\
&+ (^t\epsilon(1+At)^{-1} a\epsilon)_{k_1 l_1} (\epsilon^t a^t \epsilon (1+At)^{-1})_{l_2 k_2} \\
&+ (^t\epsilon(1+At)^{-1} a\epsilon)_{k_1 l_1} (^t\epsilon(1+At)^{-1} a\epsilon)_{k_2 l_2}) t^2)|_{t^{N/2}}, \qquad (4.24)
\end{aligned}
$$

where $H^a_{i_1 j_1 i_2 j_2}$ is the Hamiltonian matrix element $H_{i_1 j_1 i_2 j_2}$ multiplied by the matrices alpha,

$$
H^a_{k_1 l_1 k_2 l_2} = \sum_{i_1 j_1 i_2 j_2} H_{i_1 j_1 i_2 j_2} \alpha_{k_1 i_1} \alpha_{l_1 j_1} \alpha_{k_2 i_2} \alpha_{l_2 j_2}. \qquad (4.25)
$$

In the following, we introduce the following quantities $f1$-$f4$ to simplify the notation;

$$
\begin{aligned}
f1 &= {}^t\epsilon(1+At)^{-1} && (4.26)\\
f2 &= \epsilon^t a^t \epsilon (1+At)^{-1} && (4.27)\\
f3 &= \epsilon^t a^t \epsilon (1+At)^{-1} a\epsilon && (4.28)\\
f4 &= {}^t\epsilon(1+At)^{-1} a\epsilon && (4.29)
\end{aligned}
$$

With them, the energy is simplified as

$$\begin{aligned} E &= \sum_{k_1 l_1 k_2 l_2} H^a_{k_1 l_1 k_2 l_2} \frac{1}{2}\mathrm{pf}(1+At) \\ & (\frac{1}{2}((f1)_{k_2 k_1}\epsilon_{l_1 l_2} + (f1)_{k_1 k_2}\epsilon_{l_2 l_1})t \\ &- \frac{1}{2}((f2)_{l_2 k_1}(f2)_{l_1 k_2} + (f1)_{k_2 k_1}(f3)_{l_1 l_2} \\ &+ (f3)_{l_2 l_1}(f1)_{k_1 k_2} + (f4)_{k_2 l_1}(f4)_{k_1 l_2})t^2 \\ &+ \frac{1}{4}((f2)_{l_1 k_1}(f2)_{l_2 k_2} + (f2)_{l_1 k_1}(f4)_{k_2 l_2} \\ &+ (f4)_{k_1 l_1}(f2)_{l_2 k_2} + (f4)_{k_1 l_1}(f4)_{k_2 l_2})t^2)|_{t^{N/2}}. \end{aligned} \tag{4.30}$$

Computing the energy and the norm for given combination of AGP's, the total energy and the total norm are given finally as

$$E_{tot} = \sum_{xy} c_x c_y E^{xy}, \tag{4.31}$$

$$n_{tot} = \sum_{xy} c_x c_y n^{xy}. \tag{4.32}$$

$$\tag{4.33}$$

We explain how the calculation of the energy can be done with calculation steps of $O(M^5)$. We show that the following part of the energy can be calculated in $O(M^5)$ steps,

$$\sum_{k_1 l_1 k_2 l_2} H^a_{k_1 l_1 k_2 l_2} \frac{1}{2}\mathrm{pf}(1+At)(\epsilon^t a^t \epsilon (1+At)^{-1})_{l_2 k_1}(\epsilon^t a^t \epsilon (1+At)^{-1})_{l_1 k_2}. \tag{4.34}$$

The inverse of the matrix polynomial can be expressed as

$$(1+At)^{-1} = \sum_{n=0} (-1)^n A^n t^n. \tag{4.35}$$

The summation is taken up to the order of $N/2$ because we are interested in the $N/2$-th order part of the whole expression. First we take the summation

$$h_{l_1 k_2}(t) \equiv \sum_{k_1 l_2} H^a_{k_1 l_1 k_2 l_2}(\epsilon^t a^t \epsilon (1+At)^{-1})_{l_2 k_1}. \tag{4.36}$$

We can take this summation with $O(M^5)$ steps with the help of the expression (4.35). Next we take the summation

$$h'(t) \equiv \sum_{l_1 k_2} h_{l_1 k_2}(t)(\epsilon^t a^t \epsilon (1+At)^{-1})_{l_1 k_2}. \tag{4.37}$$

This summation can be taken with $O(M^4)$ steps. Finally we take the summation

$$e \equiv \{h'(t)\frac{1}{2}\mathrm{pf}(1+At)\}|_{t^{N/2}}. \tag{4.38}$$

This summation can be taken with $O(M^1)$ steps. Therefore we can calculate this part of the total energy with $O(M^5)$ steps. Other parts of the energy can be similarly calculated in $O(M^5)$ steps.

Then we switch to the description of the derivatives of the energy. In doing so, we introduce the following quantities as useful equations:

$$
\begin{aligned}
a^{xy} &= \alpha^{x\,t}\alpha^{y} && (4.39)\\
A^{xy} &= a^{xy}\epsilon^{t}a^{xy\,t}\epsilon && (4.40)\\
\frac{\partial}{\partial\alpha^{x}_{ab}}a^{xx}_{ij} &= \delta_{ai}\alpha^{x}_{jb}+\alpha^{x}_{ib}\delta_{aj} && (4.41)\\
\frac{\partial}{\partial\alpha^{x}_{ab}}a^{xy}_{ij} &= \delta_{ai}\alpha^{y}_{jb} && (4.42)\\
\frac{\partial}{\partial\alpha^{x}_{ab}}{}^{t}a^{xx}_{ij} &= \delta_{ai}\alpha^{x}_{jb}+\alpha^{x}_{ib}\delta_{aj} && (4.43)\\
\frac{\partial}{\partial\alpha^{x}_{ab}}{}^{t}a^{xy}_{ij} &= \delta_{aj}\alpha^{y}_{ib} && (4.44)\\
\frac{\partial}{\partial\alpha^{x}_{ab}}A^{xx}_{ij} &= \delta_{ai}({}^{t}\alpha^{x}\epsilon^{t}a^{xx\,t}\epsilon)_{bj}+\alpha^{x}_{ib}(\epsilon^{t}a^{xx\,t}\epsilon)_{aj}\\
&+ (a^{xx}\epsilon)_{ia}({}^{t}\alpha^{x\,t}\epsilon)_{bj}+(a^{xx}\epsilon\alpha^{x})_{ib}{}^{t}\epsilon_{aj} && (4.45)\\
\frac{\partial}{\partial\alpha^{x}_{ab}}A^{xy}_{ij} &= \delta_{ai}({}^{t}\alpha^{y}\epsilon^{t}a^{xy\,t}\epsilon)_{bj}+(a^{xy}\epsilon\alpha^{y})_{ib}{}^{t}\epsilon_{aj} && (4.46)\\
\frac{\partial}{\partial\alpha^{x}_{ab}}(1+A^{xx}t)^{-1}_{ij} &= -(1+A^{xx}t)^{-1}_{ia}({}^{t}\alpha^{x}\epsilon^{t}a^{xx\,t}\epsilon(1+A^{xx}t)^{-1})_{bj}t\\
&- ((1+A^{xx}t)^{-1}\alpha^{x})_{ib}(\epsilon^{t}a^{xx\,t}\epsilon(1+A^{xx}t)^{-1})_{aj}t\\
&- ((1+A^{xx}t)^{-1}a^{xx}\epsilon)_{ia}({}^{t}\alpha^{x\,t}\epsilon(1+A^{xx}t)^{-1})_{bj}t\\
&- ((1+A^{xx}t)^{-1}a^{xx}\epsilon\alpha^{x})_{ib}({}^{t}\epsilon(1+A^{xx}t)^{-1})_{aj}t && (4.47)\\
\frac{\partial}{\partial\alpha^{x}_{ab}}(1+A^{xy}t)^{-1}_{ij} &= -(1+A^{xy}t)^{-1}_{ia}({}^{t}\alpha^{y}\epsilon^{t}a^{xy\,t}\epsilon(1+A^{xy}t)^{-1})_{bj}t\\
&- ((1+A^{xy}t)^{-1}a^{xy}\epsilon\alpha^{y})_{ib}({}^{t}\epsilon(1+A^{xy}t)^{-1})_{aj}t && (4.48)
\end{aligned}
$$

$$
\begin{aligned}
\frac{\partial}{\partial\alpha^{y}_{ab}}a^{xy}_{ij} &= \delta_{aj}\alpha^{x}_{ib} && (4.49)\\
\frac{\partial}{\partial\alpha^{y}_{ab}}{}^{t}a^{xy}_{ij} &= \delta_{ai}\alpha^{x}_{jb} && (4.50)\\
\frac{\partial}{\partial\alpha^{y}_{ab}}A^{xy}_{ij} &= \alpha^{x}_{ib}(\epsilon^{t}a^{xy\,t}\epsilon)_{aj}+(a^{xy}\epsilon)_{ia}({}^{t}\alpha^{x\,t}\epsilon)_{bj} && (4.51)\\
\frac{\partial}{\partial\alpha^{y}_{ab}}(1+A^{xy}t)^{-1}_{ij} &= -((1+A^{xy}t)^{-1}\alpha^{x})_{ib}((\epsilon^{t}a^{xy\,t}\epsilon(1+A^{xy}t)^{-1})_{aj}t\\
&- ((1+A^{xy}t)^{-1}a^{xy}\epsilon)_{ia}({}^{t}\alpha^{x\,t}\epsilon(1+A^{xy}t)^{-1})_{bj}t && (4.52)
\end{aligned}
$$

The first derivative of the energy is provided as follows, which require the operations of $O(M^5K^2)$: For the diagonal part, or the expectation value of the Hamiltonian of the same

APG, the derivative is

$$
\begin{aligned}
\frac{\partial}{\partial \alpha^x_{ab}} E^{xx} &= \sum_{k_1 l_1 k_2 l_2} H^a_{k_1 l_1 k_2 l_2} \frac{1}{2} \mathrm{pf}(1+At) \\
& \quad (\frac{1}{2}(-(f1)_{k_2 a}({}^t\alpha^x f2)_{bk_1}(\epsilon)_{l_1 l_2} t^2 - (f1\alpha^x)_{k_2 b}(f2)_{ak_1}(\epsilon)_{l_1 l_2} t^2 \\
- & \quad (f4)_{k_2 a}({}^t\alpha^x f1)_{bk_1}(\epsilon)_{l_1 l_2} t^2 - (f4\alpha^x)_{k_2 b}(f1)_{ak_1}(\epsilon)_{l_1 l_2} t^2) \\
+ & \quad \frac{1}{2}(l_1 \leftrightarrow l_2,\ k_1 \leftrightarrow k_2) \\
- & \quad (\frac{1}{2}(\epsilon)_{l_2 a}({}^t\alpha^x f1)_{bk_1}(f2)_{l_1 k_2} t^2 + (\epsilon\alpha^x)_{l_2 b}(f1)_{ak_1}(f2)_{l_1 k_2} t^2 \\
- & \quad (f2)_{l_2 a}({}^t\alpha^x f2)_{bk_1}(f2)_{l_1 k_2} t^3 - (f2\alpha^x)_{l_2 b}(f2)_{ak_1}(f2)_{l_1 k_2} t^3 \\
- & \quad (f3)_{l_2 a}({}^t\alpha^x f1)_{bk_1}(f2)_{l_1 k_2} t^3 - (f3\alpha^x)_{l_2 b}(f1)_{ak_1}(f2)_{l_1 k_2} t^3) \\
+ & \quad \frac{1}{2}(l_1 \leftrightarrow l_2,\ k_1 \leftrightarrow k_2)) \\
+ & \quad \frac{1}{4}(l_1 \leftrightarrow l_2) \\
- & \quad \frac{1}{2}(-(f1)_{k_2 a}({}^t\alpha^x f2)_{bk_1}(f3)_{l_1 l_2} t^3 - (f1\alpha^x)_{k_2 b}(f2)_{ak_1}(f3)_{l_1 l_2} t^3 \\
- & \quad (f4)_{k_2 a}({}^t\alpha^x f1)_{bk_1}(f3)_{l_1 l_2} t^3 - (f4\alpha^x)_{k_2 b}(f1)_{ak_1}(f3)_{l_1 l_2} t^3 \\
+ & \quad (f1)_{k_2 k_1}(\epsilon)_{l_1 a}({}^t\alpha^x f4)_{bl_2} t^2 + (f1)_{k_2 k_1}(\epsilon\alpha^x)_{l_1 b}(f4)_{al_2} t^2 \\
- & \quad (f1)_{k_2 k_1}(f2)_{l_1 a}({}^t\alpha^x f3)_{bl_2} t^3 - (f1)_{k_2 k_1}(f2\alpha^x)_{l_1 b}(f3)_{al_2} t^3 \\
- & \quad (f1)_{k_2 k_1}(f3)_{l_1 a}({}^t\alpha^x f4)_{bl_2} t^3 - (f1)_{k_2 k_1}(f3\alpha^x)_{l_1 b}(f4)_{al_2} t^3 \\
+ & \quad (f1)_{k_2 k_1}(f2)_{l_1 a}({}^t\alpha^x \epsilon)_{bl_2} t^2 + (f1)_{k_2 k_1}(f2\alpha^x)_{l_1 b}(\epsilon)_{al_2} t^2) \\
- & \quad \frac{1}{2}(l_1 \leftrightarrow l_2,\ k_1 \leftrightarrow k_2) \\
- & \quad (\frac{1}{2}(-(f1)_{k_2 a}({}^t\alpha^x f3)_{bl_1}(f4)_{k_1 l_2} t^3 - (f1\alpha^x)_{k_2 b}(f3)_{al_1}(f4)_{k_1 l_2} t^3 \\
- & \quad (f4)_{k_2 a}({}^t\alpha^x f4)_{bl_1}(f4)_{k_1 l_2} t^3 - (f4\alpha^x)_{k_2 b}(f4)_{al_1}(f4)_{k_1 l_2} t^3 \\
+ & \quad (f1)_{k_2 a}({}^t\alpha^x \epsilon)_{bl_1}(f4)_{k_1 l_2} t^2 + (f1\alpha^x)_{k_2 b}(\epsilon)_{al_1}(f4)_{k_1 l_2} t^2) \\
+ & \quad \frac{1}{2}(l_1 \leftrightarrow l_2,\ k_1 \leftrightarrow k_2)) \\
+ & \quad \frac{1}{4}(k_1 \leftrightarrow k_2)
\end{aligned}
$$

$$
\begin{aligned}
+ & \quad \frac{1}{4}(\epsilon)_{l_1 a}({}^t\alpha^x f1)_{bk_1}(f4)_{k_2 l_2} t^2 + (\epsilon\alpha^x)_{l_1 b}(f1)_{ak_1}(f4)_{k_2 l_2} t^2 \\
- & \quad (f2)_{l_1 a}({}^t\alpha^x f2)_{bk_1}(f4)_{k_2 l_2} t^3 - (f2\alpha^x)_{l_1 b}(f2)_{ak_1}(f4)_{k_2 l_2} t^3 \\
- & \quad (f3)_{l_1 a}({}^t\alpha^x f1)_{bk_1}(f4)_{k_2 l_2} t^3 - (f3\alpha^x)_{l_1 b}(f1)_{ak_1}(f4)_{k_2 l_2} t^3 \\
- & \quad (f2)_{l_1 k_1}(f1)_{k_2 a}({}^t\alpha^x f3)_{bl_2} t^3 - (f2)_{l_1 k_1}(f1\alpha^x)_{k_2 b}(f3)_{al_2} t^3 \\
- & \quad (f2)_{l_1 k_1}(f4)_{k_2 a}({}^t\alpha^x f4)_{bl_2} t^3 - (f2)_{l_1 k_1}(f4\alpha^x)_{k_2 b}(f4)_{al_2} t^3 \\
+ & \quad (f2)_{l_1 k_1}(f1)_{k_2 a}({}^t\alpha^x \epsilon)_{bl_2} t^2 + (f2)_{l_1 k_1}(f1\alpha^x)_{k_2 b}(\epsilon)_{al_2} t^2) \\
+ & \quad \frac{1}{4}(l_1 \leftrightarrow l_2,\ k_1 \leftrightarrow k_2))|_{t^{N/2}}
\end{aligned}
$$

$$
\begin{aligned}
+ \quad & \frac{1}{2}\frac{1}{2}\mathrm{pf}(1+A^{xx}t)t \\
& ((^t\alpha^x f2)_{ba} + (^t\alpha^x f4)_{ba} + (f2\alpha^x)_{ab} + (f4\alpha^x)_{ab})) \\
& \sum_{k_1 l_1 k_2 l_2} H^a_{k_1 l_1 k_2 l_2} \\
& (\frac{1}{2}((f1)_{k_2 k_1}(\epsilon)_{l_1 l_2} + (f1)_{k_1 k_2}(\epsilon)_{l_2 l_1})t \\
- \quad & \frac{1}{2}((f2)_{l_2 k_1}(f2)_{l_1 k_2} + (f1)_{k_2 k_1}(f3)_{l_1 l_2} \\
+ \quad & (f3)_{l_2 l_1}(f1)_{k_1 k_2} + (f4)_{k_2 l_1}(f4)_{k_1 l_2})t^2 \\
+ \quad & \frac{1}{4}((f2)_{l_1 k_1}(f2)_{l_2 k_2} + (f2)_{l_1 k_1}(f4)_{k_2 l_2} \\
+ \quad & (f4)_{k_1 l_1}(f2)_{l_2 k_2} + (f4)_{k_1 l_1}(f4)_{k_2 l_2})t^2)|_{t^{N/2}}
\end{aligned}
$$

$$
\begin{aligned}
& + \quad \sum_{k_1 l_1 k_2 l_2} (\sum_{j_1 i_2 j_2} H_{b j_1 i_2 j_2}\delta_{k_1 a}\alpha^x_{l_1 j_1}\alpha^x_{k_2 i_2}\alpha^x_{l_2 j_2} \\
& + \quad \sum_{i_1 i_2 j_2} H_{i_1 b i_2 j_2}\alpha^x_{k_1 i_1}\delta_{l_1 a}\alpha^x_{k_2 i_2}\alpha^x_{l_2 j_2} \\
& + \quad \sum_{i_1 j_1 j_2} H_{i_1 j_1 b j_2}\alpha^x_{k_1 i_1}\alpha^x_{l_1 j_1}\delta_{k_2 a}\alpha^x_{l_2 j_2} \\
& + \quad \sum_{i_1 j_1 i_2} H_{i_1 j_1 i_2 b}\alpha^x_{k_1 i_1}\alpha^x_{l_1 j_1}\alpha^x_{k_2 i_2}\delta_{l_2 a}) \\
& \quad \frac{1}{2}\mathrm{pf}(1+At) \\
& \quad (\frac{1}{2}((f1)_{k_2 k_1}(\epsilon)_{l_1 l_2} + (f1)_{k_1 k_2}(\epsilon)_{l_2 l_1})t \\
& - \quad \frac{1}{2}((f2)_{l_2 k_1}(f2)_{l_1 k_2} + (f1)_{k_2 k_1}(f3)_{l_1 l_2} \\
& + \quad (f3)_{l_2 l_1}(f1)_{k_1 k_2} + (f4)_{k_2 l_1}(f4)_{k_1 l_2})t^2 \\
& + \quad \frac{1}{4}((f2)_{l_1 k_1}(f2)_{l_2 k_2} + (f2)_{l_1 k_1}(f4)_{k_2 l_2} \\
& + \quad (f4)_{k_1 l_1}(f2)_{l_2 k_2} + (f4)_{k_1 l_1}(f4)_{k_2 l_2})t^2)|_{t^{N/2}}. \qquad (4.53)
\end{aligned}
$$

For the off-diagonal part, the derivative is

$$
\begin{aligned}
\frac{\partial}{\partial \alpha^x_{ab}} E^{xy} &= \sum_{k_1 l_1 k_2 l_2} H^a_{k_1 l_1 k_2 l_2} \frac{1}{2} \mathrm{pf}(1+At) \\
& (\frac{1}{2}(-(f1)_{k_2 a}({}^t\alpha^y f2)_{b k_1}(\epsilon)_{l_1 l_2} t^2 \\
- & (f4\alpha^y)_{k_2 b}(f1)_{a k_1}(\epsilon)_{l_1 l_2} t^2) \\
+ & \frac{1}{2}(l_1 \leftrightarrow l_2,\ k_1 \leftrightarrow k_2) \\
- & (\frac{1}{2}((\epsilon\alpha^y)_{l_2 b}(f1)_{a k_1}(f2)_{l_1 k_2} t^2 \\
- & (f2)_{l_2 a}({}^t\alpha^y f2)_{b k_1}(f2)_{l_1 k_2} t^3 - (f3\alpha^y)_{l_2 b}(f1)_{a k_1}(f2)_{l_1 k_2} t^3) \\
+ & \frac{1}{2}(l_1 \leftrightarrow l_2,\ k_1 \leftrightarrow k_2)) \\
+ & \frac{1}{4}(l_1 \leftrightarrow l_2) \\
- & \frac{1}{2}(-(f1)_{k_2 a}({}^t\alpha^y f2)_{b k_1}(f3)_{l_1 l_2} t^3 - (f4\alpha^y)_{k_2 b}(f1)_{a k_1}(f3)_{l_1 l_2} t^3 \\
+ & (f1)_{k_2 k_1}(\epsilon\alpha^y)_{l_1 b}(f4)_{a l_2} t^2 \\
- & (f1)_{k_2 k_1}(f2)_{l_1 a}({}^t\alpha^y f3)_{b l_2} t^3 - (f1)_{k_2 k_1}(f3\alpha^y)_{l_1 b}(f4)_{a l_2} t^3 \\
+ & (f1)_{k_2 k_1}(f2)_{l_1 a}({}^t\alpha^y \epsilon)_{b l_2} t^2 \\
- & \frac{1}{2}(l_1 \leftrightarrow l_2,\ k_1 \leftrightarrow k_2) \\
- & (\frac{1}{2}(-(f1)_{k_2 a}({}^t\alpha^y f3)_{b l_1}(f4)_{k_1 l_2} t^3 - (f4\alpha^y)_{k_2 b}(f4)_{a l_1}(f4)_{k_1 l_2} t^3 \\
+ & (f1)_{k_2 a}({}^t\alpha^y \epsilon)_{b l_1}(f4)_{k_1 l_2} t^2 \\
+ & \frac{1}{2}(l_1 \leftrightarrow l_2,\ k_1 \leftrightarrow k_2)) \\
+ & \frac{1}{4}(k_1 \leftrightarrow k_2) \\
+ & \frac{1}{4}((\epsilon\alpha^y)_{l_1 b}(f1)_{a k_1}(f4)_{k_2 l_2} t^2 \\
- & (f2)_{l_1 a}({}^t\alpha^y f2)_{b k_1}(f4)_{k_2 l_2} t^3 - (f3\alpha^y)_{l_1 b}(f1)_{a k_1}(f4)_{k_2 l_2} t^3 \\
- & (f2)_{l_1 k_1}(f1)_{k_2 a}({}^t\alpha^y f3)_{b l_2} t^3 - (f2)_{l_1 k_1}(f4\alpha^y)_{k_2 b}(f4)_{a l_2} t^3 \\
+ & (f2)_{l_1 k_1}(f1)_{k_2 a}({}^t\alpha^y \epsilon)_{b l_2} t^2 \\
+ & \frac{1}{4}(l_1 \leftrightarrow l_2,\ k_1 \leftrightarrow k_2))|_{t^{N/2}}
\end{aligned}
$$

$$
\begin{aligned}
&+ \quad \frac{1}{2}\frac{1}{2}\mathrm{pf}(1+A^{xy}t)t \\
&\quad ((^t\alpha^y f2)_{ba} + (f4\alpha^y)_{ab})) \\
&\quad \sum_{k_1 l_1 k_2 l_2} H^a_{k_1 l_1 k_2 l_2} \\
&\quad (\frac{1}{2}((f1)_{k_2 k_1}(\epsilon)_{l_1 l_2} + (f1)_{k_1 k_2}(\epsilon)_{l_2 l_1})t \\
&- \quad \frac{1}{2}((f2)_{l_2 k_1}(f2)_{l_1 k_2} + (f1)_{k_2 k_1}(f3)_{l_1 l_2} \\
&+ \quad (f3)_{l_2 l_1}(f1)_{k_1 k_2} + (f4)_{k_2 l_1}(f4)_{k_1 l_2})t^2 \\
&+ \quad \frac{1}{4}((f2)_{l_1 k_1}(f2)_{l_2 k_2} + (f2)_{l_1 k_1}(f4)_{k_2 l_2} \\
&+ \quad (f4)_{k_1 l_1}(f2)_{l_2 k_2} + (f4)_{k_1 l_1}(f4)_{k_2 l_2})t^2)|_{t^{N/2}}
\end{aligned}
$$

$$
\begin{aligned}
&+ \quad \sum_{k_1 l_1 k_2 l_2} (\sum_{j_1 i_2 j_2} H_{b j_1 i_2 j_2}\delta_{k_1 a}\alpha^y_{l_1 j_1}\alpha^x_{k_2 i_2}\alpha^y_{l_2 j_2} \\
&+ \quad \sum_{i_1 j_1 j_2} H_{i_1 j_1 b j_2}\alpha^x_{k_1 i_1}\alpha^y_{l_1 j_1}\delta_{k_2 a}\alpha^y_{l_2 j_2}) \\
&\quad \frac{1}{2}\mathrm{pf}(1+At) \\
&\quad (\frac{1}{2}((f1)_{k_2 k_1}(\epsilon)_{l_1 l_2} + (f1)_{k_1 k_2}(\epsilon)_{l_2 l_1})t \\
&- \quad \frac{1}{2}((f2)_{l_2 k_1}(f2)_{l_1 k_2} + (f1)_{k_2 k_1}(f3)_{l_1 l_2} \\
&+ \quad (f3)_{l_2 l_1}(f1)_{k_1 k_2} + (f4)_{k_2 l_1}(f4)_{k_1 l_2})t^2 \\
&+ \quad \frac{1}{4}((f2)_{l_1 k_1}(f2)_{l_2 k_2} + (f2)_{l_1 k_1}(f4)_{k_2 l_2} \\
&+ \quad (f4)_{k_1 l_1}(f2)_{l_2 k_2} + (f4)_{k_1 l_1}(f4)_{k_2 l_2})t^2)|_{t^{N/2}}. \qquad (4.54)
\end{aligned}
$$

The first derivative of the norm is

$$
\begin{aligned}
\frac{\partial}{\partial \alpha^x_{ab}} n^{xx} &= \frac{1}{2}(\mathrm{pf}(1+A^{xx}t)t((^t\alpha^x f2)_{ba} + (^t\alpha^x f4)_{ba} \\
&+ \quad (f2\alpha^x)_{ab} + (f4\alpha^x)_{ab}))|_{t^{N/2}}, \qquad (4.55) \\
\frac{\partial}{\partial \alpha^x_{ab}} n^{xy} &= \frac{1}{2}(\mathrm{pf}(1+A^{xy}t)t((^t\alpha^y f2)_{ba} + (f4\alpha^y)_{ab}))|_{t^{N/2}}. \qquad (4.56)
\end{aligned}
$$

Let us explain why the calculation of the first derivatives is possible with $O(M^5)$ steps. Let us take an example for the following part

$$
\sum_{k_1 l_1 k_2 l_2} H^a_{k_1 l_1 k_2 l_2}\frac{1}{2}\mathrm{pf}(1+At)(f1)_{k_2 a}(^t\alpha^x f2)_{b k_1}(f3)_{l_1 l_2}. \qquad (4.57)
$$

For this part, we first take the summation

$$
h_{k_1 k_2}(t) \equiv \sum_{l_1 l_2} H^a_{k_1 l_1 k_2 l_2}(f3)_{l_1 l_2}. \qquad (4.58)
$$

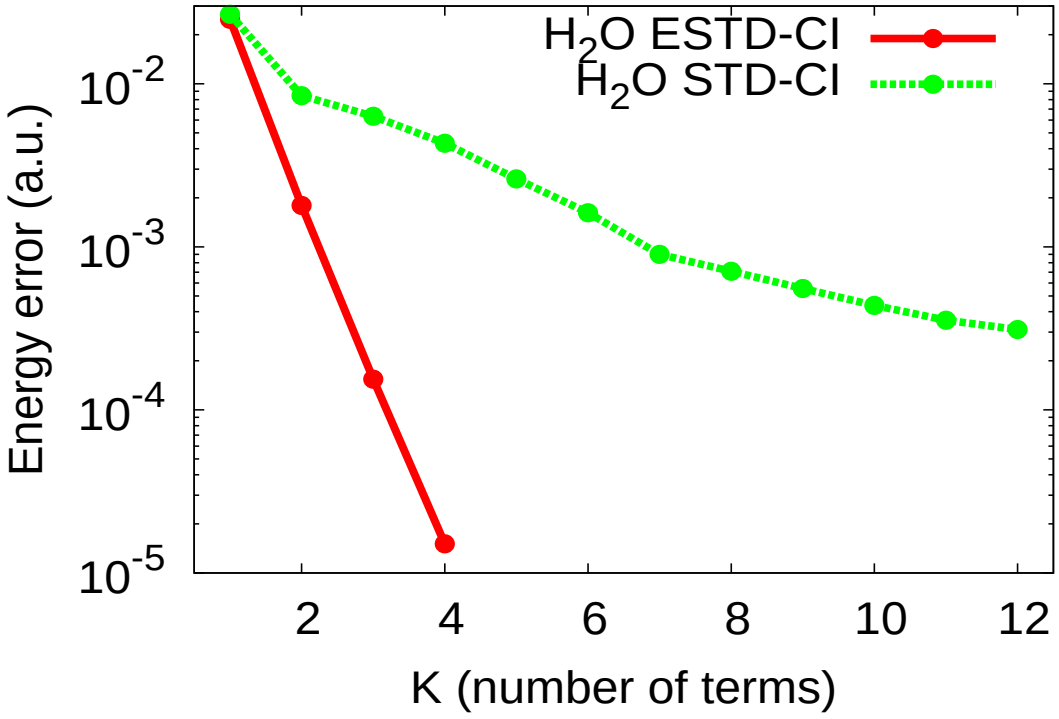

Figure 4.1: Energy error of H_2O molecule for ESTD-CI (solid line with circle) and STD-CI (broken line with circle).

This summation can be taken with $O(M^5)$ steps. Next, we take the summation

$$h'_{k_1 a}(t) \equiv \sum_{k_2} h_{k_1 k_2}(t)(f1)_{k_2 a}. \tag{4.59}$$

This summation can also be taken with $O(M^5)$ steps. Thirdly we take the summation

$$h''_{ab}(t) \equiv \sum_{k_1} h'_{k_1 a}(t)({}^t\alpha^x f2)_{b k_1}. \tag{4.60}$$

This summation can again be taken with $O(M^5)$ steps. Finally we take the following summation

$$e_{ab} \equiv \{h''_{ab}(t)\frac{1}{2}\mathrm{pf}(1+At)\}|_{t^{N/2}}. \tag{4.61}$$

This summation can be taken with $O(M^3)$ steps. Therefore we can obtain this part of the first derivative with $O(M^5)$ steps. With similar way, we can obtain other parts of the first derivatives of the energy.

4.4 Numerical Results

Figure 4.1 shows the ground state energy results of H_2O molecule with ESTD-CI and STD-CI. We are using STO-3G basis set. The geometry for this calculation is

$$O = (0, 0, 0),\ H = (-1.809, 0.0),\ (0.453549, 1.751221, 0). \tag{4.62}$$

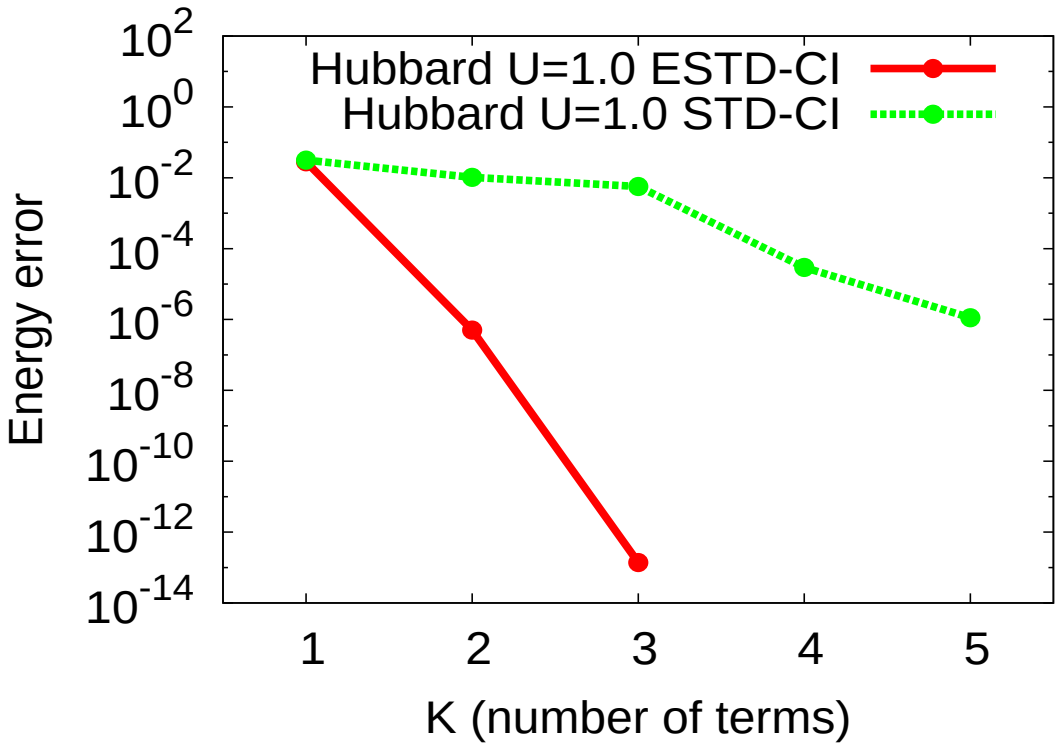

Figure 4.2: Energy error of 4 sites U=1.0 Hubbard model for ESTD-CI (solid line with circle) and STD-CI (broken line with circle).

In ESTD-CI, the convergence of the energy with respect to K is much faster than STD-CI. We used quadruple precision variables for ESTD-CI in order to maintain the numerical accuracy of the energy.

Figure 4.2, 4.3, 4.4 show the ground state energy results for 4 sites Hubbard model with ESTD-CI and STD-CI[6]. The Hubbard model is set to a condition that each pair of two sites has kinetic term. The parameter U is set to 1.0, 100.0, and 10000.0 respectively. In our results, the convergence of the energy with respect to K is again much faster in ESTD-CI than STD-CI. The calculation for the Hubbard model was done with double precision variables. We used Broyden-Fletcher-Goldfarb-Shanno algorithm (BFGS) for the variation procedure of the energy.

4.5 Discussion

The decomposition of the rank 4 Hamiltonian matrix can be possible for ESTD-CI. One can expect that when the number of terms in the decomposed Hamiltonian is L, such that

$$H_{i_1 j_1 i_2 j_2} = \sum_{i}^{L} h^{i}_{i_1 i_2} h^{i}_{j_1 j_2}, \tag{4.63}$$

Then the required steps for the energy and first order derivatives is

$$T \sim M^3 L. \tag{4.64}$$

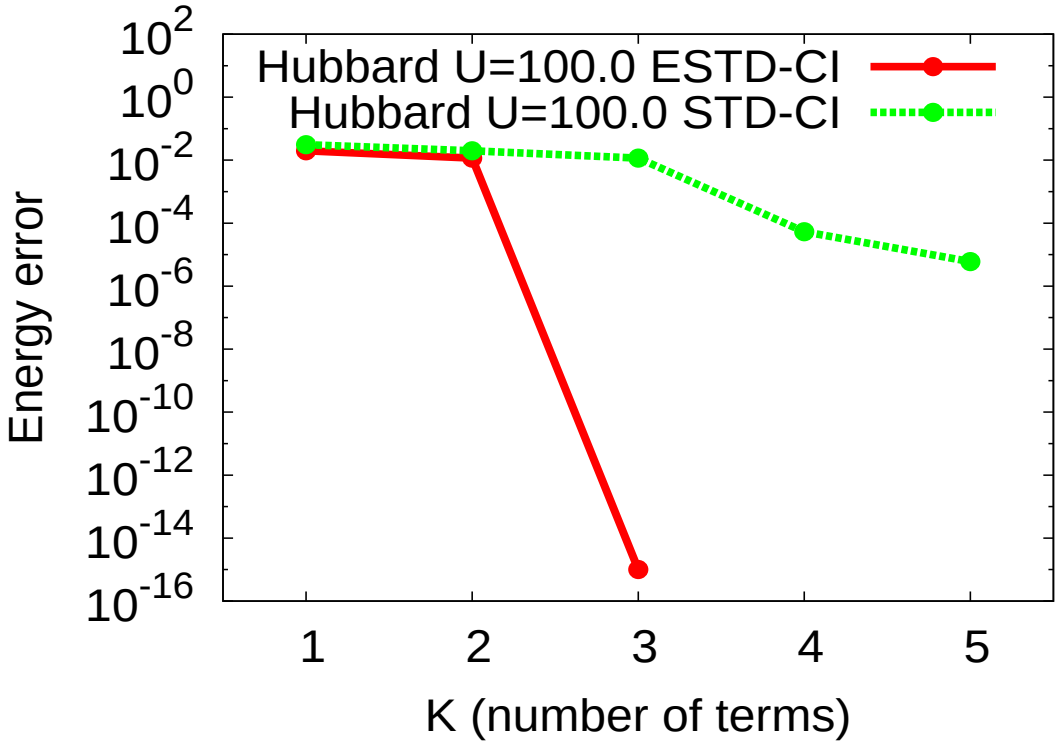

Figure 4.3: Energy error of 4 sites U=100.0 Hubbard model for ESTD-CI (solid line with circle) and STD-CI (broken line with circle).

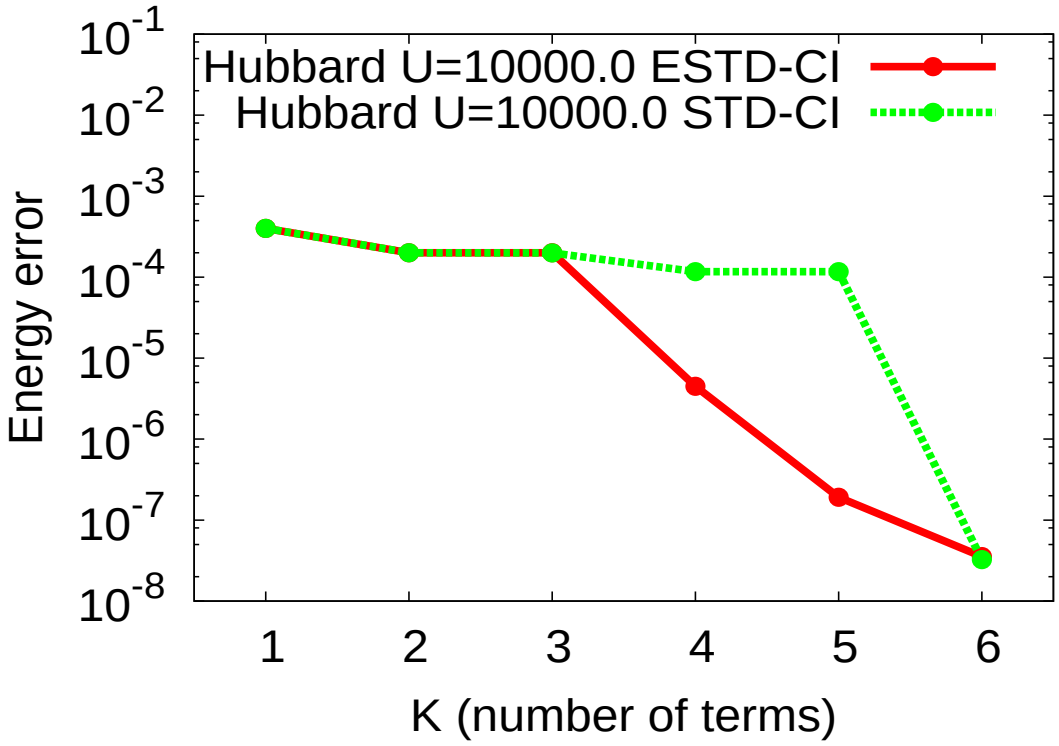

Figure 4.4: Energy error of 4 sites U=10000.0 Hubbard model for ESTD-CI (solid line with circle) and STD-CI (broken line with circle).

There are references that state the decomposition of the Hamiltonian matrix with rank 1 tensors can be reasonably possible with $L \sim M^2$. [58] Therefore we expect it is quite natural to think that L for rank 2 decomposition can be reduced to $L \sim M^1$, considering the fact that the number of variables in both decomposition is the same. If this expectation is correct, we can reduce the total cost of ESTD-CI from $T \sim M^5$ to $T \sim M^4$.

As far as we know, we need higher precision variables when we increase the number of electrons in ESTD-CI. This is partly because of the fact that we are dealing with the matrix inverse term like $(1 + At)^{-1}$ that is explicitly given by its Taylor series, including the calculation of higher powers of matrices. If we can set the size of the eigenvalue ratio of the matrix A, that is the ratio of the eigenvalue of largest absolute value and that of smallest absolute value to be fixed, then we can expect that the required precision behaves as proportional to the number of electrons. As far as we know, there are algorithms for high precision sums and products that scale as $T \sim O(n)$ and $T \sim O(n \log n \log\log n)$ respectively where n is the size of the precision. If all these statements are correct, then we can expect that the cost of ESTD-CI can behave as $T \sim M^5 K^2$.

Chapter 5

Conclusion

Recent development of DMRG and related tensor network algorithms has significantly advanced numerical research on interacting fermions. As reviewed in the introduction, those algorithms are still far from perfect and the algorithmic research is far from exhausted. The numerical success in the early DMRG theory is a sign to ensure that the tensor network language is one of the key recipes for resolving the complex and long standing puzzle of quantum many body systems, being significantly comparable to the Feynman diagrams approach, that is also a very important branch and technique of quantum many body physics. In this context, we have recognized importance in the tensor network study to explicitly involve the antisymmetry of the wavefunctions and accordingly developed two schemes for calculation. Both are based on the symmetric tensor decomposition (STD) method to decompose the symmetric part of the wavefunction into lower rank tensors. Those methods are different in the treatment of the antisymmetric part: In the STD-CI scheme the antisymmetric tensor is decomposed into product of rank-2 permutation tensors and in the ESTD-CI the tensor is decomposed into the antisymmetric sum of the products. Both methods have advantage of reducing the length of full CI series into a rapidly converging series thereby reducing the computational time significantly. In chapter 3, we demonstrated the performance of STD-CI using very small molecules, and in chapter 4, we showed that the performance is greatly improved using ESTD-CI. The ESTD-CI is equivalent to a linear combination of AGP wavefunctions and thus is a natural extension of the AGP theory. The mathematical form for ESTD-CI is quite simple and is expected as a good starting point of developing further sophisticated methods. In the future study we are planning to apply the methods to much larger systems including 3D periodic systems. In the last part of chapter 4, we suggested such development is possible when the rank reduction technique is applied to the Hamiltonian matrices because it is then possible to reduce the number of operation to $O(N^4)$ keeping a mHartree accuracy. Since $O(N^4)$ scaling is the same as that for the Hartree-Fock, such theory will indeed yield innovation in the field of computational physics.

Acknowledgments

First of all, I thank my advisor, Prof. Osamu Sugino. Through entire period of my study in ISSP, he patiently and energetically paid attention on series of my research reports. With his unchangeable support, I have managed to publish part of my research (Chapter 3) as a refereed paper. I also thank him for giving me an opportunity to attend on the CECAM workshop on Zurich, Swiss, May 2013.

I thank Dr. Yoshifumi Noguchi for his professional support on constructing the research environment with the workstation. I thank Dr. Shusuke Kasamatsu for supporting me to construct more familiar codes for STD-CI.

I thank Prof. Yuji Mochizuki and Dr. Maho Nakata for valuable discussion with the contents of Chapter 3. I thank Prof. Synge Todo for giving me an opportunity to attend on the workshop in Kobe, October 2013, that is highly encouraging one for me.

I thank all of the members of the Sugino group. I thank Dr. Yoshinari Takimoto for patiently reading my preprint and having discussion with me. I thank Dr. Takayuki Tsukagoshi. He kindly helped me to set up the research environment, including the preparation of LAPACK. He also gave us a carefully minded document about what to do with almost everything in Kashiwa. I thank Ms. Tran Hanh for continually encouraging my research. I thank Mr. Shouta Tanaka for helping me for the machine preparation. I thank Mr. Hirose Daichi for having insightful discussions. I thank Ms. Hitomi Shishido for kindly lend me her workstation for my calculation in 2013.

I thank Ms. Miyuki Onuki for kindly supported me especially when I attend the international workshop in Kashiwa, July 2012. I thank Ms. Atsuko Tsuji for supporting me when I went to workshop on abroad and attend on JPS meeting in September 2013.

Last and not least, I thank my parents and my brother. Through entire period of my research, they provided me a fundamental support of my daily live.

Tokyo, December 2013
Wataru Uemura

Bibliography

[1] S. R. White, Phys. Rev. Lett. 69, 2863 (1992).

[2] S. R. White, Phys. Rev. B 48, 10345 (1993).

[3] F. Verstraete and J. I. Cirac, Phys. Rev. B 73, 094423 (2006).

[4] G. K.-L. Chan, and M. Head-Gordon, J. Chem. Phys. 116, 4462 (2002).

[5] N. Nakatani and G. K.-L. Chan, J. Chem. Phys., 138, 134113 (2013).

[6] W. Uemura and O. Sugino, Phys. Rev. Lett. 109, 253001 (2012).

[7] U. Schollwock, Ann. Phys. (NY) 326, 96 (2011).

[8] Steven R. White and David A. Huse, Phys. Rev. B 48, 3844 (1993).

[9] F. Verstraete, D. Porras, and J. I. Cirac, Phys. Rev. Lett. 93, 227205 (2004).

[10] U. Shollwock, Rev. Mod. Phys. 77, 259 (2005).

[11] T. Xiang, J. Lou, Z. Su, Phys. Rev. B 64, 104414 (2001).

[12] O. Legaza, J. Slyom, Phys. Rev. B 70, 205118 (2004).

[13] G. Vidal, J. I. Latorre, E. Rico, A. Kitaev, Phys. Rev. Lett. 90, 227902 (2003).

[14] P. Calabrese, J. Cardy, JSTAT 0406:P06002 (2004).

[15] M. Srednicki, Phys. Rev. Lett. 71, 666 (1993).

[16] M. Plenio, J. Eisert, J. Dreiig, M. Cramer, Phys. Rev. Lett. 94, 060503 (2005).

[17] R. Orus, arXiv:1306.2164v2.

[18] F. Verstraete, M. M. Wolf, D. Perez-Garcia, and J. I. Cirac, Phys. Rev. Lett. 96, 220601 (2006).

[19] E. Cuthill and J. McKee, in Proceedings of the 24th National Conference of the ACM, 1969.

[20] J. Liu and A. Sherman, SIAM (Soc. Ind. Appl. Math.) J. Numer. Anal. 13, 198 (1975).

[21] R. Bartlett, J. Watts, S. Kucharski, and J. Noga, Chem. Phys. Lett. 165, 513 (1990).

[22] J.P. Bouchaud and C. Lhuillier, Europhys. Lett. 3, 1273 (1987).

[23] S.M. Bhattacharjee, Z. Phys. B 82, 323 (1991).

[24] M. Bajdich, L. Mitas, G. Drobn, L. K. Wagner and K. E. Schmidt, Phys. Rev. Lett. 96, 130201 (2006).

[25] M. Bajdich, L. Mitas, L. K. Wagner and K. E. Schmidt, Phys. Rev. B 77, 115112 (2008).

[26] B.L. Hammond, W.A. Lester Jr., and P.J. Reynolds, Monte Carlo Methods in ab initio Quantum Chemistry (World Scientific, Singapore, 1994).

[27] M.W.C. Foulkes, L. Mitas, R.J. Needs, and G. Rajagopal, Rev. Mod. Phys. 73, 33 (2001).

[28] C.J. Umrigar, K.G. Wilson, and J.W. Wilkins, Phys. Rev. Lett. 60, 1719 (1988).

[29] C.J. Umrigar and C. Filippi, Phys. Rev. Lett. 94, 150201 (2005).

[30] D. Bressanini, D.M. Ceperley, and P. Reynolds, in Recent Advances in Quantum Monte Carlo Methods II, edited by W.A. Lester, S.M. Rothstein, and S. Tanaka (World Scientific, Singapore, 2002).

[31] D. Bressanini and P.J. Reynolds, Phys. Rev. Lett. 95, 110201 (2005).

[32] I. Shavitt, Mol. Phys., 94, 3 (1998).

[33] J. Cízek, J. Chem. Phys., 45, 4256 (1966); Adv. Chem. Phys., 14, 35 (1969).

[34] J. Cízek and J. Paldus, Int. J. Quantum Chem., 5, 359 (1971).

[35] M. Nakata, H. Nakatsuji et al., J. Chem. Phys. 116, 5432 (2002).

[36] S. Rommer and S. Ostlund, Phys. Rev. B 55, 2164 (1997).

[37] S. Daul, I. Ciofini, C. Daul and Steven R. White, Int. J. Quant. Chem. 79, 331(2000).

[38] S. Sharma and G. K-L. Chan, J. Chem. Phys. 136, 124121 (2012).

[39] K. H. Marti, B. Bauer, M. Reiher, M. Troyer and F. Verstraete, New J. Phys., 12, 103008 (2010).

[40] K. H. Marti and M. Reiher, Phys. Chem. Chem. Phys., 13, 6750 (2011).

[41] F. Hitchcock, J. Math. Phys. 6, 164 (1927); *ibid* 7, 9 (1927).

[42] L. R. Tucker, Psychometrika 31, 279 (1966).

[43] J. D. Carroll and J. J. Chang, Psychometrika, 35, 283 (1970).

[44] R. A. Harshman, UCLA Working Papers in Phonetics, 16, 1 (1970).

[45] F. Bell, D. S. Lambrecht and M. Head-Gordon, Mol. Phys. 108, 2759 (2010).

[46] U. Benedikt, A. A. Auer, M. Espig, and W. Hackbusch, J. Chem. Phys. 134, 054118 (2011).

[47] D.C. Kay, "Tensor Calculus. Schaum's Outlines", McGraw Hill (USA) (1988),

[48] F. Viète, Opera mathematica, edited by F. van Schooten p. 162 (1579). Reprinted Leiden, Netherlands (1646).

[49] M. Hasse, J. Appl. Math. Mech., 40, 523 (1960).

[50] N. E. Brener and J. L. Fry, Phys. Rev. B17, 506 (1978).

[51] J. L. Fry, N. E. Brener, and R. K. Bruyere, Phys. Rev. B16, 5225 (1977).

[52] T. van Mourik, A. K. Wilson and T. H. Dunning JR, Mol. Phys., 96, 529 (1999).

[53] U. Kleinekathofer, K.T. Tang, J.P. Toennies and C.L. Yiu, Chem. Phys. Lett., 249, 257(1996).

[54] K. Kitaura, E. Ikeo, T. Asada, T. Nakano and M. Uebayasi, Chem. Phys. Lett., 313, 701 (1999).

[55] Kh. D. Ikramov, H. Fassbender, J. Math. Sci., 157, 5, 697 (2009).

[56] A. J. Coleman, Rev. Mod. Phys. 35, 668 (1963).

[57] A. J. Coleman, J. Math. Phys. 6, 1425 (1965).

[58] Udo Benedikt, Alexander A. Auer, Mike Espig and Wolfgang Hackbusch, J. Chem. Phys. 134, 054118 (2011).